Inorg. Chem. **2009**, *48*, 3591−3607

Low-Energy Bands of Ferrocene−Ferrocenium Dimers: Bandshape Analysis with a Four-Level Two-Mode Vibronic Coupling Configuration Interaction (VCCI) Model Including Asymmetry

Ralf Warratz and Felix Tuczek*

Institut für Anorganische Chemie, Christian Albrechts Universität Kiel, Max Eyth Strasse 2, D-24098 Kiel, Germany

Received November 4, 2008

Ferrocene−ferrocenium dimers exhibit a double-peak intervalence charge-transfer (IVCT) band in the NIR/MIR region, which is analyzed in terms of a four-level, two-mode vibronic coupling configuration interaction (VCCI) scheme. Besides providing satisfactory fits of the measured spectra, the model also gives electronic and vibronic coupling parameters as well as CI mixing coefficients. A temperature-dependent asymmetry of the potential is introduced in order to describe the temperature dependence of the solid-state spectra and account for complementary Mössbauer data, which indicate a temperature-driven electron localization−delocalization transition in the singly bridged radical cations. The VCCI model is also successfully applied to the doubly bridged Fe(II)−Fe(III) bisfulvalenide dimer, which exhibits a double-peak IVCT transition as well. The VCCI analysis reveals that all dimers have a one-minimum potential in the ground state, leading in the absence of asymmetry to class III behavior (electron delocalization). If electron localization corresponding to class II characteristics occurs, it is due to an asymmetric (but still one-minimum) potential and not, as usual, to a double-minimum potential, explaining the class II−III borderline behavior observed for these systems.

1. Introduction

The dependence of electron-transfer rates on small geometric changes is of interest in all areas of chemistry, biology, and physics.[1] A class of small-molecule compounds that has proven to be particularly well-suited for the study of this subject includes Fe(II)−Fe(III) mixed-valent (MV) bimetallocenes.[2−9] As initially discovered by Mössbauer spectroscopy,[3] these systems in the solid state undergo a thermally driven change from charge localization to charge delocalization. This phenomenon may be exemplified on ferrocenyl−ferrocenium (biferrocenyl) triiodide, $\mathbf{Fc_2I_3}$ (actually $\mathbf{Fc_2^{\bullet+}I_3^-}$; **1**) and 1′-1‴-diethylbiferrocenyl triiodide, $\mathbf{(FcEt)_2I_3}$; **2**).

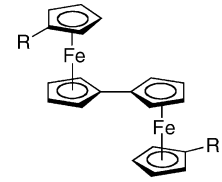

R=H : $\mathbf{Fc_2}$
R=Et: $\mathbf{(FcEt)_2}$

The parent system $\mathbf{Fc_2I_3}$ is charge-localized between 4.2 and 300 K, exhibiting two discrete quadrupole doublets for Fe(II) and Fe(III) in the Mössbauer spectrum. At $T_c = 360$ K, a transition to a charge-delocalized state occurs, which is evident from the appearance of a single quadrupole doublet.[10,11] For $\mathbf{(FcEt)_2I_3}$, a corresponding charge locali-

* To whom correspondence should be addressed. E-mail: ftuczek@ac.uni-kiel.de.

(1) (a) Solomon, E. I.; Xie, X. J.; Dey, A. *Chem. Soc. Rev.* **2008**, *37*, 623. (b) Page, C. C.; Moser, C. C.; Dutton, L. P. *Curr. Opin. Chem. Biol.* **2003**, *7*, 551–556. (c) *Electron Transfer in Chemistry and Biology*; Kuznetsov, A., Ulstrup, J., Eds.; Wiley-VCH: New York, 1998. (d) *Electron Transfer in Biology and the Solid State: Inorganic Compounds with Unusual Properties (Adv. in Chemistry Ser)*; King, R. B., Johnson, M. K., Kurtz, D. M., Kutal, C., Norton, M. L., Scott, R. A., Eds.; Oxford University Press: New York, 1989.
(2) (a) Barlow, S.; O'Hare, D. *Chem. Rev.* **1997**, *97*, 637. (b) Jones, S. C.; Barlow, S.; O'Hare, D. *Chem.—Eur. J.* **2005**, *11*, 4473.
(3) Hendrickson, D. N. *NATO Sci. Ser., Ser. C* **1991**, *343*, 67.
(4) Sano, H. *Hyperfine Interact.* **1990**, *53*, 97.
(5) Dong, T.-Y.; Chang, L.-S.; Lee, G.-H.; Peng, S.-M. *Organometallics* **2002**, *21*, 4192.
(6) Oda, T.; Nakashima, S.; Okuda, T. *Inorg. Chem.* **2003**, *42*, 5376.
(7) Morrison, W. H., Jr.; Hendrickson, D. N. *Inorg. Chem.* **1975**, *14*, 2331.
(8) Jones, S. C.; Barlow, S.; O'Hare, D. *Chem.—Eur. J.* **2005**, *11*, 4473.
(9) Richardson, D. E.; Taube, H. *Coord. Chem. Rev.* **1984**, *60*, 107.
(10) Iijiama, S.; Saida, R.; Motoyama, I.; Sano, H. *Bull. Chem. Soc. Jpn.* **1981**, *54*, 1375.

10.1021/ic802112h CCC: $40.75
Published on Web 03/25/2009

zation−delocalization transition is observed at $T_c = 275$ K. In the vibronic model of Varret and co-workers, which has further been elaborated by Klokishner et al.,[12] these transitions have been attributed to cooperative interactions between the bimetallocene molecules in the crystalline solid which modulate the energy difference W_d between the local minima of the double-well potentials of the individual dimers. At or above T_c, the energy difference W_d becomes zero, and the Fe(II)−Fe(III) units behave as symmetric class II−III mixed-valent dimers according to the Robin and Day classification scheme.[13,14] In the presence of fast relaxation (which always applies to these systems),[12] a *charge-delocalized* state exhibiting, for example, *one* Mössbauer doublet is observed. Below T_c, the potential becomes asymmetric, and W_d may become large compared to kT, effectively leading to a *charge-ordered* state. In this case, two distinct Mössbauer doublets are observed, one mostly deriving from Fe(III) and the other one mostly from Fe(II).

An important spectroscopic tool used to obtain information about the electronic structure of MV systems is the detection and analysis of intervalence charge-transfer (IVCT) bands.[15,16] An IVCT transition has been detected for biferrocenyl cations and has been interpreted on the basis of the Piepho−Krausz−Schatz (PKS) model.[17] However, no temperature dependence was recorded, and no satisfactory fit of the absorption band was obtained.[18] We therefore decided to reinvestigate the radical cations of **Fc_2** and **$(FcEt)_2$** by means of optical absorption spectroscopy, both in the solid state and in solution. In a recent publication, UV/vis/NIR/MIR absorption spectra of these two systems were presented.[19] Importantly, the solution spectra of **$Fc_2^{\bullet+}$** and **$(FcEt)_2^{\bullet+}$** in addition to the known NIR band (band Ib) revealed the presence of another low-energy transition in the MIR (band Ia) which had been unknown to date (Figure 1). Moreover, both bands exhibited solvent shifts, with that of band Ib being more pronounced than that of band Ia. About the same spectrum was observed when the neutral Fe(II)−Fe(II) dimer **Fc_2** was deposited by evaporation into an Ar matrix and ionized by X-ray radiation.[19] On the basis of DFT calculations, both the new absorption feature and the known absorption band in the NIR were assigned to IVCT (or charge-resonance) transitions.[20] Specifically, band Ia was assigned to the transition between the symmetric and antisymmetric combination of the $d_{x^2-y^2}$ orbitals on the two iron centers, whereas band Ib was attributed to a transition from a lower-lying antisymmetric combination of d_{z^2} orbitals to the symmetric combination of $d_{x^2-y^2}$ orbitals, heavily mixing with the first transition. The two components of band II were assigned to the transition from the highest-energy ligand orbital to the semioccupied molecular orbital (SOMO) of **$Fc_2^{\bullet+}$** ("hole transition") and the SOMO−LUMO (LUMO = lowest unoccupied molecular orbital) transition of this radical cation.[19]

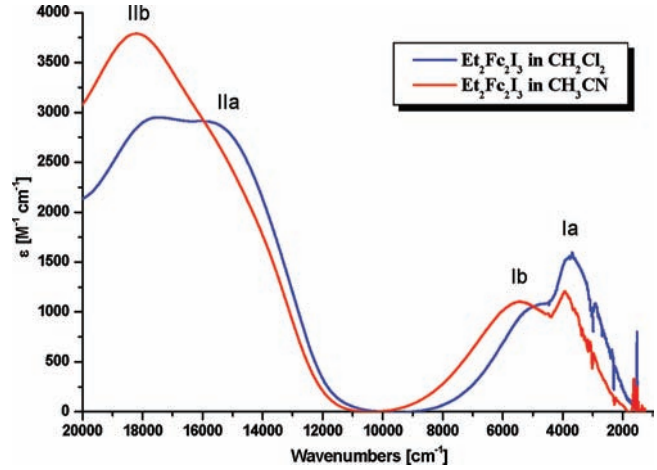

Figure 1. Low-energy bands of 1′,1‴-diethylbiferrocenyl triiodide (**$(FcEt)_2I_3$**) in dichloromethane and acetonitrile (300 K).

Herein, the temperature-dependent solid-state spectra of **Fc_2I_3** and **$(FcEt)_2I_3$** are presented and analyzed. In order to simulate the band shape of the observed two-peak IVCT transition, a vibronic coupling configuration interaction (VCCI) scheme is developed. This approach is based on the PKS model, which successfully has been employed to analyze IVCT transitions of a variety of MV dimers.[15,21] Whereas the original PKS model only includes one orbital on each metal, the VCCI model takes into account two orbitals on each subunit, which can mix by configuration interaction, as required to describe the situation in the Fe(II)−Fe(III) bimetallocenes. Furthermore, the original PKS model only includes local vibrational modes on the two metal subunits. Later on, the model was expanded by Piepho[22] to include molecular vibrations as, for example, the subunit−subunit stretching mode, which becomes more relevant when the system becomes more delocalized.[23] In fact, in order to optimize the fit of the temperature-dependent spectra of the present study, it appeared necessary to include a second active mode. As evident from the above discussion, another key parameter is asymmetry, which in the original PKS model has been taken into account by an off-diagonal matrix element. In a more recent treatment by Gasyna et al.,[24] asymmetry was treated by configuration interaction. Here,

(11) Nakashima, S.; Nishimori, A.; Masuda, Y.; Sano, H.; Sorai, M. *J. Phys. Chem. Solids* **1991**, *52*, 1169.
(12) Klokishner, S.; Linares, J.; Varret, F. *Chem. Phys.* **1998**, *226*, 171.
(13) Robin, M. B.; Day, P. *Adv. Inorg. Chem. Radiochem.* **1967**, *10*, 247.
(14) Wong, K. Y.; Schatz, P. N. *Prog. Inorg. Chem.* **1981**, *28*, 369.
(15) Brunschwig, B. S.; Creutz, C.; Sutin, N. *Chem. Soc. Rev.* **2002**, *31*, 168.
(16) Schatz, P. N. In *Inorganic Electronic Structure and Spectroscopy*; Solomon, E. I., Lever, A. B. P., Eds.; J. Wiley: New York, 1999.
(17) Piepho, S. B.; Krausz, E. R.; Schatz, P. N. *J. Am. Chem. Soc.* **1978**, *100*, 2996.
(18) Talham, D. R.; Cowan, D. O. *Organometallics* **1984**, *3*, 1712.
(19) Warratz, R.; Aboulfadl, H.; Bally, Th.; Tuczek, F. *Chem. Eur. J.* **2009**, *15*, 1604.
(20) In the case of a class III dimer, there is no net charge transfer, and the term "intervalence charge transfer transition" for the low-energy electronic transition within the symmetric/antisymmetric pair of MOs containing the SOMO of a radical is, strictly speaking, wrong. Badger and Brocklehurst had proposed the term "charge resonance" band some time ago for such a transition: Badger, B.; Brocklehurst, B. *Trans. Faraday Soc.* **1969**, 2576.
(21) Schatz, P. N. In *Inorganic Electronic Structure and Spectroscopy, Volume II: Applications and Case Studies*; Solomon, E. I., Lever, A. B. B., Eds.; John Wiley & Sons: New York, 1990; S. 175.
(22) Piepho, S. B. *J. Am. Chem. Soc.* **1988**, *110*, 6319.
(23) Reimers, J. R.; Hush, N. S. *Chem. Phys.* **1996**, *208*, 177.
(24) Gasyna, Z.; Schatz, P. N.; Boyle, M. E. *J. Phys. Chem.* **1995**, *99*, 10159.

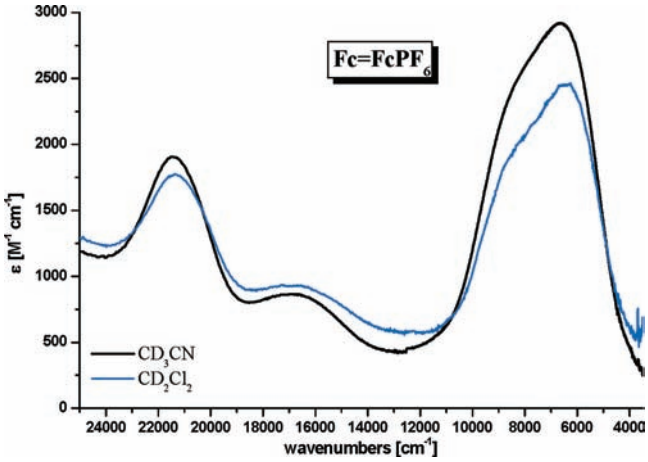

Figure 2. Vis−NIR spectra of **Fc=FcPF$_6$** in acetonitrile and dichloromethane.

both the formalism of Gasyna and Schatz and the PKS treatment of asymmetry are applied and compared to each other, as suggested by Schatz.[21]

For comparison with the singly bridged ferrocenyl ferrocenium compounds **1** and **2**, the doubly bridged ferrocenylene ferrocenylenium system (Fe(II)Fe(III) bisfulvalenide ≡ **(Fc=Fc$^{\bullet+}$)I$_3$**; **3**) was investigated in the previous study as well. Importantly, Mössbauer spectroscopy showed that the bisfulvalenide diiron cation is always delocalized, and no localization−delocalization transitions exist in this type of molecule.

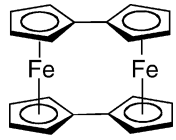

Fc=Fc

As evident from Figure 2, this compound also exhibits a double-peak, low-energy IVCT band in its optical absorption spectrum, which had been known in the literature.[7,18,25,26] In this case, no solvent shifts are observed. In the preceding paper, the electronic structure of this radical cation was evaluated by DFT calculations as well and compared with that of the singly bridged counterparts, showing stronger electronic coupling between the two metallocene units.[19] Herein, the temperature-dependent solid-state spectra of this dimer are also investigated and analyzed with the four-level two-mode VCCI model, relating the derived parameters to those obtained on the singly bridged systems. The general implications of the experimental and theoretical results with respect to electron localization and delocalization in mixed-valent Fe(II)−Fe(III) bimetallocenes are discussed.

(25) LeVanda, C.; Bechgaard, K.; Cowan, D. O.; Mueller-Westerhoff, U. T.; Eilbracht, P.; Candela, G. A.; Collins, R. L. *J. Am. Chem. Soc.* **1976**, *98*, 3181.
(26) Mueller-Westerhoff, U. T.; Eilbracht, P. *J. Am. Chem. Soc.* **1972**, *94*, 9272.
(27) Ko, J.; Zhang, L.-T.; Ondrechen, M. *J. Am. Chem. Soc.* **1986**, *108*, 1712.

Scheme 1. Simplified MO Model of Mixed-Valent Biferrocenes with Splitting Parameters

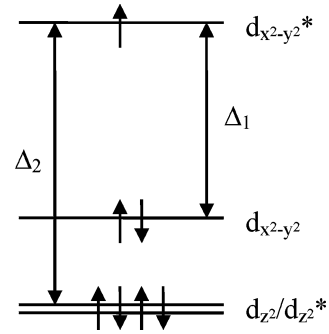

2. Theory

A. Simplified MO Scheme of Ferrocene Ferrocenium Dimers. For the evaluation of the IVCT transitions of the singly and doubly bridged ferrocene ferrocenium dimers, the MO schemes obtained by the DFT calculations of the preceding paper are reduced to a set of four orbitals (cf. Scheme 1 and Figure 3). The SOMO of both mixed-valent dimers is the cp−cp antibonding combination of the subunit $d_{x^2-y^2}$ orbitals, which has a_g symmetry in the biferrocenyl cations **Fc$_2^{\bullet+}$** and **(FcEt)$_2^{\bullet+}$** and b_{1u} symmetry in the Fe(II)−Fe(III) bisfulvalenide cation **Fc=Fc$^{\bullet+}$**. The doubly occupied, bonding combination of these orbitals having b_u symmetry for **Fc$_2^{\bullet+}$** and a_g symmetry for **Fc=Fc$^{\bullet+}$** is separated from the SOMO by an energy difference Δ_1 which corresponds to the respective bonding/antibonding interaction. Below the pair of $d_{x^2-y^2}$ functions, the nearly degenerate pair of d_{z^2} combinations is located, which has a_g/b_u symmetry for **Fc$_2^{\bullet+}$** and b_{1u}/a_g symmetry for **Fc=Fc$^{\bullet+}$**. These doubly occupied orbitals are separated from the SOMO by an energy difference Δ_2. Excitation of one electron from one of the doubly occupied orbitals to the SOMO leads to three excited electronic states, φ_2^0, φ_3^0, and φ_4^0, which together with the ground state φ_1^0 make up the four electronic basis states of the VCCI model.

B. Vibronic Coupling Configuration Interaction (VCCI) Model. In order to account for the presence of more than two electronic states involved in IVCT transitions, a four-state vibronic coupling model including configuration interaction is employed. This model is based on the PKS model,[14,17] which in its original version contains two electronic states coupled by an electronic interaction 2ε. The vibrational modes originally considered by PKS are the symmetric and antisymmetric combination of totally symmetric subunit stretching vibrations, denoted as the Q_+^{loc} and Q_-^{loc} modes, respectively (cf Scheme 2):

Scheme 2. Representation of the Antisymmetric (Q_-), Symmetric (Q_+), and Molecular (Q_{AB}) Vibrational Modes of Biferrocene

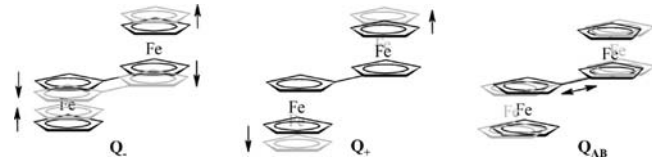

Here, Q_A and Q_B are the coordinates of the symmetric metal−ligand stretching vibration of one subunit. Later,

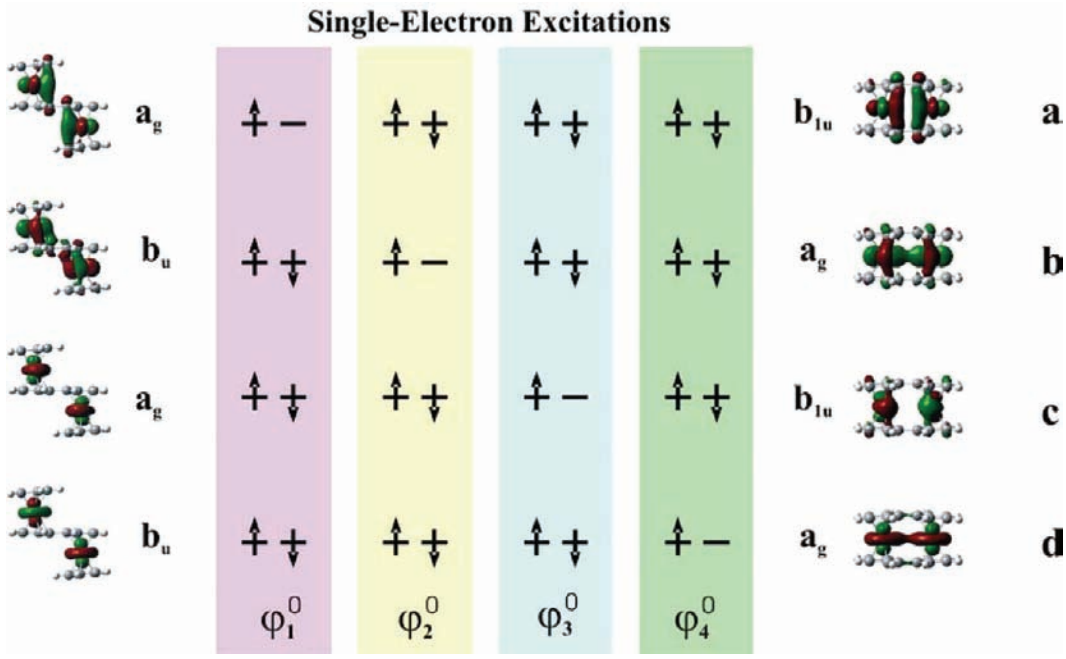

Figure 3. Possible low-energy single-electron excitations for singly (left) and doubly (right) bridged mixed-valent ferrocene−ferrocenium dimers.

Ondrechen et al.[27−29] showed that especially in delocalized systems other molecular modes become relevant. The most important mode in this respect is the Q_{AB} mode, which describes the vibration of the subunits against each other:

$$Q_+^{loc} = (1/\sqrt{2})(Q_A + Q_B), \quad Q_-^{loc} = (1/\sqrt{2})(Q_A - Q_B) \qquad (1)$$

$$Q_+^{molec} = Q_{AB} \qquad (2)$$

In localized systems, vibronic coupling in the Q_- mode will be dominant. In this case, one electron is transferred from one metal center of the dimer to the other side, corresponding to an interchange of the respective oxidation states and bond lengths. In delocalized systems, on the other hand, when one electron is transferred from a delocalized bonding orbital into a delocalized antibonding orbital, the coupling of the Q_{AB} mode will be strong. An estimate of the magnitude of these vibronic couplings has been provided by Piepho,[22,30,31] using Bersuker's[32] orbital vibronic constants (OVC; see below). The Q_+^{loc} mode, finally, is not involved in vibronic interactions and thus separates from the problem.

We follow Piepho and consider a symmetric system being composed of two centers, A and B, of different oxidation states, connected by a bridge. The relevant molecular orbitals are the bonding and antibonding combination of the highest-occupied subunit orbitals. The bonding combination of these orbitals (*b*) is fully occupied, whereas the antibonding (*a*) combination is singly occupied. Furthermore, we have two additional excited states where one electron is transferred from a lower-lying set of orbitals (*c* and *d*) that is fully occupied and possibly also split by a bonding/antibonding interaction (cf Figure 3, right). The *a* and *c* as well as the *b* and *d* combinations have the same symmetries, and the resulting electronic states are

$$\varphi_1^0 = |d^2c^2b^2a^1\rangle, \varphi_2^0 = |d^2c^2b^1a^2\rangle,$$
$$\varphi_3^0 = |d^2c^1b^2a^2\rangle, \varphi_4^0 = |d^1c^2b^2a^2\rangle \qquad (3)$$

In the case of the ferrocene−ferrocenium dimers, the individual MOs are given by (cf. Figure 3 and Scheme 1)

$$|a\rangle = (1/\sqrt{2})(e_2'(A) \pm e_2'(B)), \; |b\rangle = (1/\sqrt{2})(e_2'(A) \mp e_2'(B))$$
$$|c\rangle = (1/\sqrt{2})(a_1'(A) \pm a_1'(B)), \; |d\rangle = (1/\sqrt{2})(a_1'(A) \mp a_1'(B)) \qquad (4)$$

Here, e_2'(A) and e_2'(B) are the highest-occupied subunit orbitals in the D_{5h} point group and a_1'(A) and a_1'(B) lie below these orbitals. The upper and lower signs refer to the singly and doubly bridged dimers, respectively.

On the basis of the corresponding energy differences in the MO scheme (see preceding paper[19] and Scheme 1), the energetic difference between the *a* and *b* states is given by the electronic interaction Δ_1, whereas the separation of states *c* and *d* to the ground state is given by Δ_2. The electronic interaction between states *c* and *d* is neglected at the zeroth order since these orbitals are nearly degenerate. However, the states φ_1^0 and φ_3^0 as well as φ_2^0 and φ_4^0 can mix by configuration interaction ζ, which gives rise to a splitting between φ_3^0 and φ_4^0.

Now we consider the two active vibrational modes introduced above:

$$Q_+^{molec} = Q_{AB} \equiv Q_1, Q_-^{loc} = (1/\sqrt{2})(Q_A - Q_B) \equiv Q_2 \qquad (5)$$

(28) Zhang, L.-T.; Ko, J.; Ondrechen, M. *J. Am. Chem. Soc.* **1987**, *109*, 1666.
(29) Ondrechen, M.; Ko, J.; Zhang, L.-T. *J. Am. Chem. Soc.* **1987**, *109*, 1672.
(30) Piepho, S. B. *J. Am. Chem. Soc.* **1990**, *112*, 4197.
(31) Piepho, S. B. Vibronic Coupling Models for Mixed Valence Line Shapes: Going beyond the PKS Approach. In *Mixed Valency Systems: Applications in Chemistry, Physics and Biology*; Prassides, K., Ed.; Kluver: Dordrecht, The Netherlands, 1991; p 329.
(32) Bersuker, I. B. *The Jahn Teller Effect and Vibronic Interactions in Modern Chemistry*;Plenum: New York, 1984.

The total Hamiltonian for a molecular system including these vibrations is given by[14,17,22]

$$\hat{H}_T(r, Q) = \hat{H}_{el}(r, Q) + \hat{T}_N(Q) \quad (6)$$

where r and Q are electronic and nuclear coordinates and

$$\hat{H}_{el}(r, Q) = \hat{T}_e(r) + \hat{V}_{ee}(r) + \hat{V}(r, Q) \quad (7)$$

where $\hat{T}_N$ and $\hat{T}_e$ are the nuclear and electronic kinetic operators, $\hat{V}_{ee}$ is the electron−electron interaction, and $\hat{V}(r,Q)$ is the vibronic electron−nuclear operator. The zeroth-order electronic functions ($\phi_j(r,Q) \equiv \phi_j^0$) satisfy the condition

$$H_{el}(r, Q)\, \varphi_j^0 = W_j^0(Q_0)\varphi_j^0 \quad (8)$$

at the ground-state equilibrium configuration $Q_0 = 0$.

We want to solve the dynamic Schrödinger equation

$$\hat{H}_T\Psi_k = E_k\Psi_k \quad (9)$$

To this end, the wave functions Ψ_k are expanded in the basis[14,17,22]

$$\varphi_j^0\chi_{n_1}^1\chi_{n_2}^2 \quad j = 1, ..., 4; n_1 = 1, 2, ...; n_2 = 1, 2, ... \quad (10)$$

where the $\chi_{ni}{}^i$ are oscillator functions associated with the normal coordinates Q_i. The vibronic-coupling CI (VCCI) matrix for $\hat{H}_T$ in the $\varphi_j{}^0$ basis is then given by

$$\begin{bmatrix} T_N + W_1^0 + W_{11} & W_{12} & \zeta & \\ W_{21} & T_N + W_2^0 + W_{22} & & \zeta \\ \zeta & & T_N + W_3^0 + W_{33} & W_{34} \\ & \zeta & W_{43} & T_N + W_4^0 + W_{44} \end{bmatrix} \quad (11)$$

where ζ is a configuration interaction matrix element and

$$W_{jj}(Q) = \sum_{\alpha=1}^{2} (l_\alpha^{(j)}Q_\alpha + 1/2k_\alpha^{(j)}Q_\alpha^2) \quad (12)$$

$$W_{j=1,j'=2}(Q) = W_{j=3,j'=4}(Q) = \sum_{\alpha=1}^{4} l_\alpha^{(j,j')}Q_\alpha \quad (13)$$

with the other W_{ij} being 0. The linear vibronic coupling terms l and the force constants k are given by

$$l_\alpha^{(j)} = \langle\varphi_j^0|\left(\frac{\partial V}{\partial Q_\alpha}\right)_0|\varphi_j^0\rangle,\ l_\alpha^{(j,j')} = \langle\varphi_j^0|\left(\frac{\partial V}{\partial Q_\alpha}\right)_0|\varphi_{j'}^0\rangle,$$
$$k_\alpha^{(j)} = \langle\varphi_j^0|\left(\frac{\partial^2 V}{\partial Q_\alpha^2}\right)_0|\varphi_j^0\rangle \quad (14)$$

respectively. Using the dimensionless variables

$$q_\alpha \equiv (\sqrt{h\nu_\alpha}/\hbar)Q_\alpha \text{ and } \lambda_\alpha \equiv \frac{\hbar}{\sqrt{2}h\nu_\alpha\sqrt{h\nu_\alpha}}l_\alpha \quad (15)$$

with $\nu_\alpha = (1/2\pi)\sqrt{k_\alpha}$ as the fundamental vibrational frequency connected to the Q_α coordinate and assuming that $k_\alpha{}^{(1)} = k_\alpha{}^{(2)} = k_\alpha{}^{(3)} = k_\alpha{}^{(4)}$, we get

$$W_{jj}(q) = \sum_{\alpha=1}^{2} h\nu_\alpha[\sqrt{2}\lambda_\alpha^{(j)}q_\alpha + (1/2)q_\alpha^2] \quad (16)$$

and

$$W_{jj'}(q) = \sqrt{2}\sum_{\alpha=1}^{2} h\nu_\alpha\lambda_\alpha^{(j,j')}q_\alpha \quad (17)$$

Note that for symmetry reasons W_{11}, W_{22}, W_{33}, and W_{44} contain no linear terms in q_2:

$$\langle\varphi_i^0|(\partial V/\partial q_2)_0|\varphi_i^0\rangle = 0, i = 1, 2, 3, 4 \quad (18)$$

and W_{12} and W_{34} and contain no linear terms in q_1:

$$\langle\varphi_i^0|(\partial V/\partial q_1)_0|\varphi_j^0\rangle = 0, i \neq j = 1, 2, 3, 4 \quad (19)$$

C. Expansion to the Asymmetric Case. Up to now, the model is only valid for symmetric dimers with A = B. We now expand the model to dimers that contain metal centers in slightly different environments. This will be achieved via two different methods, by introducing a configuration interaction and an off-diagonal matrix element.

Inclusion of Asymmetry As a Configuration Interaction Following Gasyna et al.[24] We include a small asymmetry element that results in a slight difference between the two metal centers. In fact, we mix the molecular orbitals a and b as well as c and d by means of a configuration interaction which gives new molecular orbitals (a', b', c', and d') and new electronic states ($\varphi_1{}'^0$, $\varphi_2{}'^0$, $\varphi_3{}'^0$, and $\varphi_4{}'^0$)

$$\varphi_1'^0 = |a'^1b'^2c'^2d'^2\rangle,\ \varphi_2'^0 = |a'^2b^1c'^2d'^2\rangle,$$
$$\varphi_3'^0 = |a'^2b'^2c'^1d'^2\rangle,\ \varphi_4'^0 = |a'^2b'^2c'^2d'^1\rangle \quad (20)$$

where

$$|a'\rangle = \eta_1|a\rangle - \eta_2|b\rangle,\ |b'\rangle = \eta_1|b\rangle + \eta_2|a\rangle$$
$$|c'\rangle = \eta_1|c\rangle - \eta_2|d\rangle,\ |d'\rangle = \eta_1|d\rangle + \eta_2|c\rangle \quad (21)$$

with

$$\eta_1^2 + \eta_2^2 = 1,\ |\eta_1| \gg |\eta_2| \quad (22)$$

We may write eqs 16 and 17 in the form:

$$W_{ii}(q) = (1/2)h\nu_1q_1^2 + \sqrt{2}\lambda_1^{(i)}h\nu_1q_1 + (1/2)h\nu_2q_2^2 + \sqrt{2}\lambda_2^{(i)}h\nu_2q_2 \text{ for } i = 1, 2, 3, 4 \quad (23)$$

$$W_{12}(q) = W_{21}(q) = \sqrt{2}\lambda_1^{(1,2)}h\nu_1q_1 + \sqrt{2}\lambda_2^{(1,2)}h\nu_2q_2 \quad (24)$$

and

$$W_{34}(q) = W_{43}(q) = \sqrt{2}\lambda_1^{(3,4)}h\nu_1q_1 + \sqrt{2}\lambda_2^{(3,4)}h\nu_2q_2 \quad (25)$$

Here,

$$\sqrt{2}\lambda_{\alpha}^{(i)} h\nu_{\alpha} = \langle \varphi_i'^0 | \left(\frac{\partial V}{\partial q_{\alpha}}\right)_0 | \varphi_i'^0 \rangle,\ i = 1, 2, 3, 4 \tag{26}$$

$$\sqrt{2}\lambda_{\alpha}^{(1,2)} h\nu_{\alpha} = \langle \varphi_1'^0 | \left(\frac{\partial V}{\partial q_{\alpha}}\right)_0 | \varphi_2'^0 \rangle \text{ and } \sqrt{2}\lambda_{\alpha}^{(3,4)} h\nu_{\alpha} = \langle \varphi_3'^0 | \left(\frac{\partial V}{\partial q_{\alpha}}\right)_0 | \varphi_4'^0 \rangle,\ \alpha = 1, 2 \tag{27}$$

When Bersuker is followed,[33] the $(\partial V/\partial q_{\alpha})_0$ are a sum of one-electron operators:

$$\left(\frac{\partial V}{\partial q_{\alpha}}\right)_0 = \sum_i \left(\frac{\partial v(i)}{\partial q_{\alpha}}\right)_0 \tag{28}$$

We thus expand the matrix elements 26 and 27 to one-electron terms using eqs 20 and 21, leading to

$$\begin{aligned}
h\nu_2\lambda_2^{(1)} &= -h\nu_2\lambda_2^{(2)} = \eta_1\eta_2\left[\langle e_2'(\mathrm{A})|\left(\frac{\partial v(i)}{\partial q_{\mathrm{A}}}\right)_0 |e_2'(\mathrm{A})\rangle - \langle e_2'(\mathrm{A})|\left(\frac{\partial v(i)}{\partial q_{\mathrm{B}}}\right)_0 |e_2'(\mathrm{A})\rangle\right] \\
h\nu_1(\lambda_1^{(2)} - \lambda_1^{(1)}) &= \sqrt{2}(\eta_2^2 - \eta_1^2)\langle e_2'(\mathrm{A})\left(\frac{\partial v(i)}{\partial q_1}\right)_0 \Big| e_2'(\mathrm{A})\rangle \\
h\nu_1\lambda_1^{(1,2)} &= \sqrt{2}\eta_1\eta_2\langle e_2'(\mathrm{A})\Big|\left(\frac{\partial v(i)}{\partial q_1}\right)_0 \Big| e_2'(\mathrm{B})\rangle \\
h\nu_2\lambda_2^{(1,2)} &= 1/2(\eta_1^2 - \eta_2^2)\left[\langle e_2'(\mathrm{A})\Big|\left(\frac{\partial v(i)}{\partial q_{\mathrm{A}}}\right)_0 \Big| e_2'(\mathrm{A})\rangle - \langle e_2'(\mathrm{A})|\left(\frac{\partial v(i)}{\partial q_{\mathrm{B}}}\right)_0 |e_2'(\mathrm{A})\rangle\right]
\end{aligned} \tag{29}$$

and, correspondingly,

$$\begin{aligned}
h\nu_2\lambda_2^{(3)} &= -h\nu_2\lambda_2^{(4)} = \eta_1\eta_2\left[\langle a_1'(\mathrm{A})|\left(\frac{\partial v(i)}{\partial q_{\mathrm{A}}}\right)_0 |a_1'(\mathrm{A})\rangle - \langle a_1'(\mathrm{A})|\left(\frac{\partial v(i)}{\partial q_{\mathrm{B}}}\right)_0 |a_1'(\mathrm{A})\rangle\right] \\
h\nu_1(\lambda_1^{(4)} - \lambda_1^{(3)}) &= \sqrt{2}(\eta_2^2 - \eta_1^2)\langle a_1'(\mathrm{A})|\left(\frac{\partial v(i)}{\partial q_1}\right)_0 |a_1'(\mathrm{A})\rangle \\
h\nu_1\lambda_1^{(3,4)} &= \sqrt{2}\eta_1\eta_2\langle a_1'(\mathrm{A})|\left(\frac{\partial v(i)}{\partial q_1}\right)_0 |a_1'(\mathrm{B})\rangle \\
h\nu_2\lambda_2^{(3,4)} &= 1/2(\eta_1^2 - \eta_2^2)\left[\langle a_1'(\mathrm{A})|\left(\frac{\partial v(i)}{\partial q_{\mathrm{A}}}\right)_0 |a_1'(\mathrm{A})\rangle - \langle a_1'(\mathrm{A})|\left(\frac{\partial v(i)}{\partial q_{\mathrm{B}}}\right)_0 |a_1'(\mathrm{A})\rangle\right]
\end{aligned} \tag{30}$$

By inspection of eqs 29 and 30, it is found that

$$\frac{\lambda_2^{(1)}}{2\lambda_2^{(1,2)}} = -\frac{\lambda_2^{(2)}}{2\lambda_2^{(1,2)}} = \frac{\lambda_1^{(1,2)}}{\lambda_1^{(2)}} = \frac{\lambda_2^{(3)}}{2\lambda_2^{(3,4)}} = -\frac{\lambda_2^{(4)}}{2\lambda_2^{(3,4)}} = \frac{\eta_1\eta_2}{\eta_2^2 - \eta_1^2} \equiv R \tag{31}$$

Furthermore, we set

$$\lambda_1^{(1)} = 0,\ \lambda_1^{(4)} - \lambda_1^{(3)} = 0, \text{ and } \lambda_1^{(3,4)} = 0 \tag{32}$$

The first relation holds as the ground state is in equilibrium with respect to Q_1. The last two relations are approximately true, as $\varphi_3'^0$ and $\varphi_4'^0$ are electronically weakly coupled, and thus no *intrinsic* vibronic coupling with Q_1 is expected. However, we need to allow for a possible vertical displacement of both $\varphi_3'^0$ and $\varphi_4'^0$ with respect to $\varphi_1'^0$.

As a result, we get the following Hamiltonian (cf. eq 11):

$$\begin{bmatrix}
(1/2)q_1^2 h\nu_1 + (1/2)q_2^2 h\nu_2 + 2\sqrt{2}R\lambda_1^{(2)} q_1 h\nu_1 & \sqrt{2}R\lambda_1^{(2)} q_1 h\nu_1 + \sqrt{2}\lambda_2^{(1,2)} q_2 h\nu_2 & \zeta & \\
\sqrt{2}R\lambda_1^{(2)} q_1 h\nu_1 + \sqrt{2}\lambda_2^{(1,2)} q_2 h\nu_2 & \Delta_1 + (1/2)q_1^2 h\nu_1 + (1/2)q_2^2 h\nu_2 + \sqrt{2}\lambda_1^{(2)} q_1 h\nu_1 - 2\sqrt{2}R\lambda_2^{(1,2)} q_2 h\nu_2 & & \zeta \\
\zeta & & \Delta_2 + (1/2)q_1^2 h\nu_1 + (1/2)q_2^2 h\nu_2 + \sqrt{2}\lambda_1^{(3)} q_1 h\nu_1 + 2\sqrt{2}R\lambda_2^{(3,4)} q_2 h\nu_2 & \sqrt{2}\lambda_2^{(3,4)} q_2 h\nu_2 \\
 & \zeta & \sqrt{2}\lambda_2^{(3,4)} q_2 h\nu_2 & \Delta_2 + (1/2)q_1^2 h\nu_1 + (1/2)q_2^2 h\nu_2 + \sqrt{2}\lambda_1^{(3)} q_1 h\nu_1 - 2\sqrt{2}R\lambda_2^{(3,4)} q_2 h\nu_2
\end{bmatrix} \tag{33}$$

The solution to the dynamic Schrödinger equation (eq 9) is now obtained by diagonalizing the corresponding dynamic matrix in the $\phi_{jn_1n_2} = \varphi_j'^0\ \chi_{n_1}(q_1)\ \chi_{n_2}(q_2)$ basis. Evaluation of eq 33 in this basis gives the following diagonal elements:

$$\begin{aligned}
\langle\phi_{1n_1n_2}|\hat{H}_T|\phi_{1n_1n_2}\rangle &= \sum_{i=1}^{2}(n_i + 1/2)h\nu_i \\
\langle\phi_{2n_1n_2}|\hat{H}_T|\phi_{2n_1n_2}\rangle &= \Delta_1 + \sum_{i=1}^{2}(n_i + 1/2)h\nu_i \\
\langle\phi_{3n_1n_2}|\hat{H}_T|\phi_{3n_1n_2}\rangle &= \Delta_2 + \sum_{i=1}^{2}(n_i + 1/2)h\nu_i \\
\langle\phi_{4n_1n_2}|\hat{H}_T|\phi_{4n_1n_2}\rangle &= \Delta_2 + \sum_{i=1}^{2}(n_i + 1/2)h\nu_i
\end{aligned} \tag{34}$$

as well as the following off-diagonal elements:

$$\begin{aligned}
\langle\phi_{1n_1n_2}|\hat{H}_T|\phi_{2n_1n_2'}\rangle &= \langle\phi_{2n_1,n_2}|\hat{H}_T|\phi_{1n_1,n_2'}\rangle = \sqrt{2}h\nu_2\lambda_2^{(1,2)}\left[\left(\frac{n_2+1}{2}\right)^{1/2}\delta_{n_2',n_2+1} + \left(\frac{n_2'+1}{2}\right)^{1/2}\delta_{n_2,n_2'+1}\right] \\
\langle\phi_{3n_1n_2}|\hat{H}_T|\phi_{4n_1n_2'}\rangle &= \langle\phi_{4n_1,n_2}|\hat{H}_T|\phi_{3n_1,n_2'}\rangle = \sqrt{2}h\nu_2\lambda_2^{(3,4)}\left[\left(\frac{n_2+1}{2}\right)^{1/2}\delta_{n_2',n_2+1} + \left(\frac{n_2'+1}{2}\right)^{1/2}\delta_{n_2,n_2'+1}\right] \\
\langle\phi_{2n_1n_2}|\hat{H}_T|\phi_{2n_1'n_2}\rangle &= \sqrt{2}h\nu_1\lambda_1^{(2)}\left[\left(\frac{n_1+1}{2}\right)^{1/2}\delta_{n_1',n_1+1} + \left(\frac{n_1'+1}{2}\right)^{1/2}\delta_{n_1,n_1'+1}\right] \\
\langle\phi_{3n_1n_2}|\hat{H}_T|\phi_{3n_1'n_2}\rangle &= \langle\phi_{4n_1n_2}|\hat{H}_T|\phi_{4n_1'n_2}\rangle = \sqrt{2}h\nu_1\lambda_1^{(3)}\left[\left(\frac{n_1+1}{2}\right)^{1/2}\delta_{n_1',n_1+1} + \left(\frac{n_1'+1}{2}\right)^{1/2}\delta_{n_1,n_1'+1}\right]
\end{aligned} \tag{35}$$

Furthermore, we get off-diagonal elements for $\zeta \neq 0$:

$$\begin{aligned}
\langle\phi_{1n_1n_2}|\hat{H}_T|\phi_{3n_1n_2}\rangle &= \zeta \\
\langle\phi_{2n_1n_2}|\hat{H}_T|\phi_{4n_1n_2}\rangle &= \zeta
\end{aligned} \tag{36}$$

Asymmetry of the two metal centers ($A \neq B$; $R \neq 0$) leads to the following additional terms:

$$\begin{aligned}
\langle\phi_{1n_1n_2}|\hat{H}_T|\phi_{1n_1n_2'}\rangle &= -\langle\phi_{2n_1n_2}|\hat{H}_T|\phi_{2n_1n_2'}\rangle = 2\sqrt{2}Rh\nu_2\lambda_2^{(1,2)}\left[\left(\frac{n_2+1}{2}\right)^{1/2}\delta_{n_2',n_2+1} + \left(\frac{n_2'+1}{2}\right)^{1/2}\delta_{n_2,n_2'+1}\right] \\
\langle\phi_{3n_1n_2}|\hat{H}_T|\phi_{3n_1n_2'}\rangle &= -\langle\phi_{4n_1n_2}|\hat{H}_T|\phi_{4n_1n_2'}\rangle = 2\sqrt{2}Rh\nu_2\lambda_2^{(3,4)}\left[\left(\frac{n_2+1}{2}\right)^{1/2}\delta_{n_2',n_2+1} + \left(\frac{n_2'+1}{2}\right)^{1/2}\delta_{n_2,n_2'+1}\right] \\
\langle\phi_{1n_1n_2}|\hat{H}_T|\phi_{2n_1'n_2}\rangle &= \langle\phi_{2n_1n_2}|\hat{H}_T|\varphi_{1n_1'n_2}\rangle = \sqrt{2}Rh\nu_1\lambda_1^{(2)}\left[\left(\frac{n_1+1}{2}\right)^{1/2}\delta_{n_1',n_1+1} + \left(\frac{n_1'+1}{2}\right)^{1/2}\delta_{n_1,n_1'+1}\right]
\end{aligned} \tag{37}$$

Inclusion of Asymmetry Based on the PKS Model. The dissimilarity of the two metal centers resulting in an asymmetry with different zero-point energies had already been included in the original PKS model. Assuming that the difference in coordination spheres is small, such that the force constants differ only slightly, asymmetry can be introduced using an off-diagonal matrix element. We use the same vibronic basis, leading to identical diagonal elements, as in the symmetric case with additional off-diagonal elements W_2^{As} and W_4^{As}. This results in the following matrix for the Hamiltonian:

$$\begin{bmatrix}
(1/2)q_1^2h\nu_1 + (1/2)q_2^2h\nu_2 & \sqrt{2}\lambda_2^{(1,2)}q_2h\nu_2 + W_2^{As} & \zeta & \\
\sqrt{2}\lambda_2^{(1,2)}q_2h\nu_2 + W_2^{As} & \Delta_1 + (1/2)q_1^2h\nu_1 + (1/2)q_2^2h\nu_2 + \sqrt{2}\lambda_1^{(2)}q_1h\nu_1 & & \zeta \\
\zeta & & \Delta_2 + (1/2)q_1^2h\nu_1 + (1/2)q_2^2h\nu_2 + \sqrt{2}\lambda_1^{(3)}q_1h\nu_1 & \sqrt{2}\lambda_2^{(3,4)}q_2h\nu_2 + W_4^{As} \\
 & \zeta & \sqrt{2}\lambda_2^{(3,4)}q_2h\nu_2 + W_4^{As} & \Delta_2 + (1/2)q_1^2h\nu_1 + (1/2)q_2^2h\nu_2 + \sqrt{2}\lambda_1^{(4)}q_1h\nu_1
\end{bmatrix} \tag{38}$$

Asymmetry, as introduced in this manner, has the effect of a static distortion along the Q–coordinate, $q_2 \rightarrow q_2 - q_2^0$, with $q_2^0 \neq 0$. For the off-diagonal matrix elements, we then have

$$\sqrt{2}\lambda_2^{(i,j)}q_2h\nu_2 \rightarrow \sqrt{2}\lambda_2^{(i,j)}q_2h\nu_2 - \sqrt{2}\lambda_2^{(i,j)}q_2^0h\nu_2 \equiv \sqrt{2}\lambda_2^{(i,j)}q_2h\nu_2 + W_j^{As} \tag{39}$$

Therefore, we set

$$W_4^{As} = W_2^{As}\frac{\lambda_2^{(3,4)}}{\lambda_2^{(1,2)}} \quad (40)$$

3. Band Shape Analysis

Both the interaction matrixes 33 and 38 are diagonalized, giving eigenfunctions

$$\Psi_k = \sum_j \varphi_j^0 \sum_{n_1 n_2} r^k_{jn_1n_2}\chi^1_{n_1}\chi^2_{n_2} \quad (41)$$

Electric dipole matrix elements between these vibronic eigenfunctions are then evaluated by projecting out the respective $\varphi_1{}^0$ and $\varphi_2{}^0$ contributions:

$$\langle\Psi_k|\underline{\mu}|\Psi_{k'}\rangle = \sum_n r^k_{1n_1n_2}r^{k'}_{2n_1n_2}\langle\varphi_1^0|\underline{\mu}|\varphi_2^0\rangle + r^k_{2n_1n_2}r^{k'}_{1n_1n_2}\langle\varphi_2^0|\underline{\mu}|\varphi_1^0\rangle \quad (42)$$

That is, the ($\varphi_1{}^0 \rightarrow \varphi_2{}^0$) transition is considered as the only IVCT-intensity-generating mechanism, borrowing intensity to the forbidden $\varphi_1{}^0 \rightarrow (\varphi_3{}^0, \varphi_4{}^0)$ transitions by configuration interaction.

Before fitting the intervalence bands, the optical solid-state spectra are approximated by a Gaussian deconvolution followed by subtraction of the band assigned to the interdimer transition.[19] The residual absorption profile is fitted by a band shape resulting from diagonalization of the four-level, two-mode VCCI matrices 33 and 38.[33] In the resulting level scheme, all possible transitions from occupied to unoccupied levels are considered, weighted with a Boltzmann factor of the respective occupied level. Knowledge of the eigenfunctions 41 then allows calculation of the dipole strengths via the matrix elements 42. Summation of all individual vibronic transitions leads to a stick spectrum. Each stick is convoluted with a Gaussian of line width Γ to give the theoretical absorption profile, which is then compared with the experimental absorption spectrum.

The following parameters enter the spectral simulation: (1) the electronic splitting of the $d_{x^2-y^2}$ orbitals, Δ_1, which corresponds to $2\varepsilon h\nu_-$, ε being the electronic coupling parameter of the two-state PKS model; (2) the separation of the d_{z^2} orbitals from the $d_{x^2-y^2}$ orbitals, Δ_2; (3) the electronic mixing coefficient between $d_{x^2-y^2}$ and d_{z^2} orbitals, ζ; (4) the vibronic coupling parameter $\lambda_1{}^{(2)} \equiv \lambda_1$, which determines the vertical displacement of the excited $d_{x^2-y^2}$ state with respect to the $d_{x^2-y^2}$ ground state; (5) the vibronic coupling parameter $\lambda_2{}^{(1,2)} \equiv \lambda_2$, which determines the degree of vibronic coupling in the $d_{x^2-y^2}$ states and corresponds to the coupling constant λ of the two-state PKS model; (6) the corresponding parameter for the excited d_{z^2} states, $\lambda_2{}^{(3,4)} \equiv \lambda_4$; and, finally, (7) the vibronic coupling parameter $\lambda_1{}^{(3)} = \lambda_1{}^{(4)} \equiv \lambda_3$, which determines the vertical displacement of the d_{z^2} with respect to the $d_{x^2-y^2}$ states. In total, therefore, we have three electronic interaction parameters and four vibronic coupling constants (two in Q_1 and two in Q_2). In addition, the vibrational frequencies ν_1 and ν_2 of the $Q_1 = Q_{AB}$ and the $Q_2 = Q_-$ modes have to be known. On the basis of the infrared and Raman spectra of the mixed-valent cations, their neutral precursors, and ferrocene, the value for the stretching frequencies ν_1 is set to 506 cm^{-1} for **Fc_2I_3**, 502 cm^{-1} for **$(FcEt)_2I_3$**, and 525 cm^{-1} for **$(Fc{=}Fc^{\bullet+})I_3$**, whereas the value for ν_2 is set to 310 cm^{-1} for all compounds (cf. Supporting Information).

The large number of variables involved in the theoretical analysis renders the determination of an optimal parameter set a highly complex task (an exploration of the parameter space is given in the Supporting Information) Apart from the stretching frequencies ν_1 and ν_2, which are fixed, initial values for all parameters are estimated from the spectra and then optimized by trial and error to give a best fit. An additional restriction of parameter space is imposed by the temperature dependence of the spectra; here, the spectra are fitted at low as well as at high temperatures using identical parameters with the exception of the asymmetry parameters R (Gasyna and Schatz) and W_i^{As} (PKS), respectively, which are set to 0 at room temperature and to a nonvanishing value at low temperatures (see below).

It has to be kept in mind, however, that an asymmetric potential in either treatment reduces the integral absorption of the IVCT band. To see this in the Gasyna and Schatz formalism, we consider the perturbed $d_{x^2-y^2}$ functions $\varphi_1{}'^0$ and $\varphi_2{}'^0$. With eqs 21 and 31, $\eta_1 \approx 1$, $\eta_2 \ll \eta_1$, and $R \approx -\eta_1$, we have

$$|a'\rangle = \sqrt{1-R^2}|a\rangle + R|b\rangle \quad |b'\rangle = \sqrt{1-R^2}|b\rangle - R|a\rangle \quad (43)$$

Therefore,

$$\langle a'|\underline{\mu}|b'\rangle = (1-2R^2)\langle a|\underline{\mu}|b\rangle \quad (44)$$

and the intensities of the individual vibronic transitions are correspondingly reduced by a factor of $(1-2R^2)^2$, which is reflected by an overall decrease of the integral absorption by the same amount. In the PKS treatment of asymmetry, on the other hand, $\varphi_1{}^0$ and $\varphi_2{}^0$ interact via the matrix element W_2^{As}. Correspondingly, the wave functions mix in the first order by a coefficient W_2^{As}/Δ_1, which has a similar effect on the electric-dipole matrix elements and the corresponding intensities as the coefficient R.

A comparison of the experimentally measured spectra for **Fc_2I_3** (compound **1**) and those resulting from the VCCI model with the asymmetry treated according to Gasyna and Schatz is shown in Figure 4; the corresponding parameters are collected in Table 1. For the vibronic coupling in the pseudo Jahn−Teller-active mode Q_-, a value of $\lambda_2 = 1.10$ is obtained. The position of the lower-energy band leads to an electronic interaction parameter Δ_1 of 3000 cm^{-1}. These parameters, together with an asymmetry parameter $R = 0$ at room temperature, correspond to a potential energy surface of the $d_{x^2-y^2}$ ground state with a single minimum (Figure 5) and a probability distribution with a maximum at $Q_- = 0$, indicating a symmetric class III configuration of the mixed-valent dimer.

For the d_{z^2} excited states, the coupling in the antisymmetric Q_- mode is represented by $\lambda_4 = 1.15$, which is

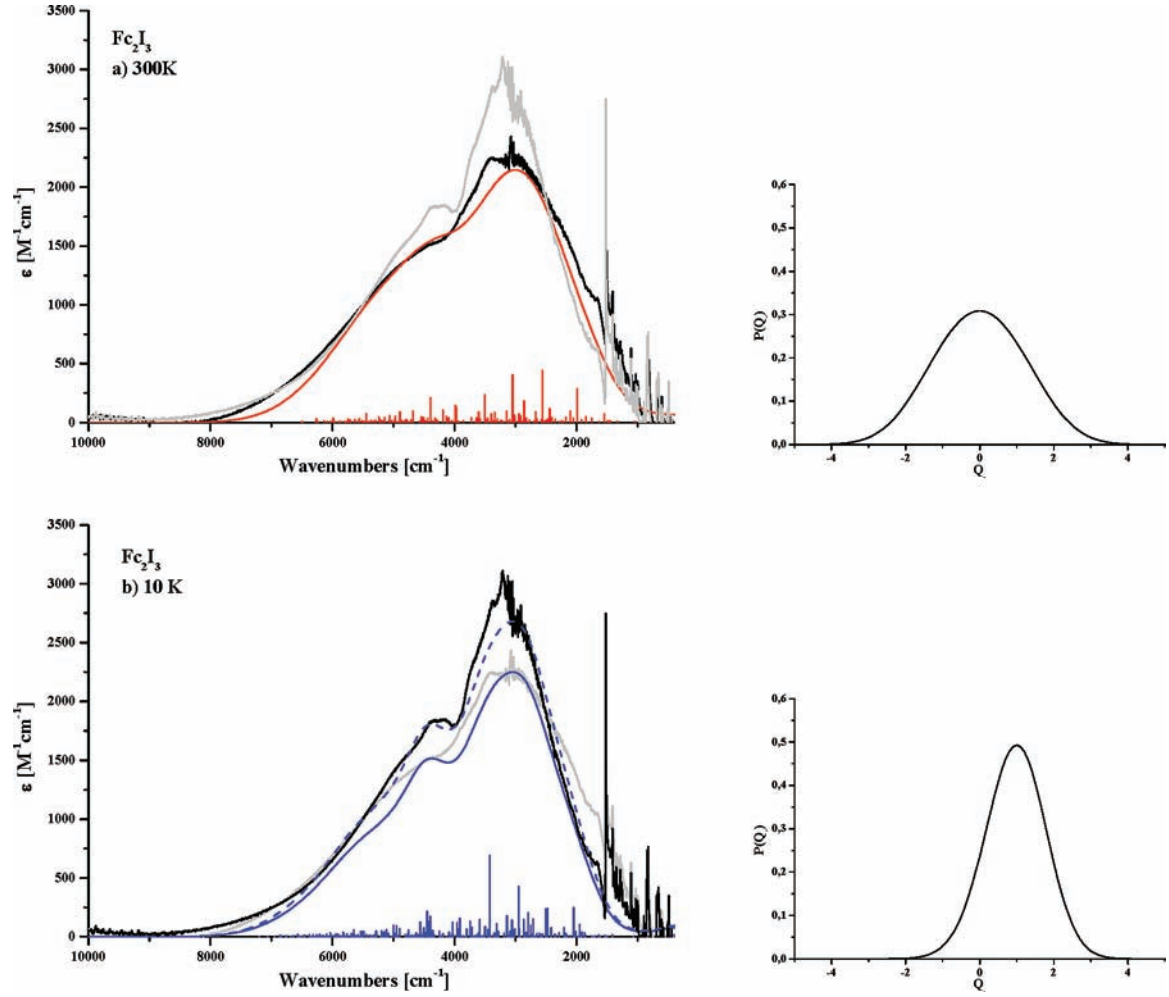

Figure 4. Low-energy optical band of biferrocenyl triiodide (**1**) with theoretical fits (treatment of asymmetry following Gasyna and Schatz). (a) $T = 300$ K (black: experimental spectrum; red: theoretical spectrum; gray: experimental spectrum at 10 K) and (b) $T = 10$ K (black: experimental spectrum; blue: theoretical spectrum; dashed blue: theoretical spectrum scaled by $f_1 = 1.19$; gray: experimental spectrum at 300 K). Right: probability distribution ($P(Q_-)$). See text and Table 1 for details.

Table 1. Fitting Parameters Using the Four-State VCCI Model; Vibrational Frequencies are $h\nu_- = 310$ for all compounds and $h\nu_+ = 506$ cm^{-1} for **Fc_2I_3**, 502 cm^{-1} for **$Et_2Fc_2I_3$**, and 525 cm^{-1} for **$(Fc{=}Fc^{\bullet+})I_3$**

fitting parameters (Gasyna and Schatz)											
compd	Δ_1 [cm^{-1}]	Δ_2 [cm^{-1}]	λ_1	λ_2	λ_3	λ_4	ζ [cm^{-1}]	Γ_{300K} [cm^{-1}]	Γ_{10K} [cm^{-1}]	R_{300K}	R_{10K}
Fc_2I_3	3000	4600	−2.00	1.10	−0.55	1.15	700	550	450	0.00	0.14
$Et_2Fc_2I_3$	2900	4950	−1.50	1.00	−0.30	1.35	500	450	350	0.00	0.14

fitting parameters (PKS)											
compd	Δ_1 [cm^{-1}]	Δ_2 [cm^{-1}]	λ_1	λ_2	λ_3	λ_4	ζ [cm^{-1}]	Γ_{300K} [cm^{-1}]	Γ_{10K} [cm^{-1}]	W_{300K} [cm^{-1}]	W_{10K} [cm^{-1}]
Fc_2I_3	3000	4850	−1.90	1.10	−0.55	1.15	700	550	450	0	350
$Et_2Fc_2I_3$	2800	5250	−1.55	1.10	−0.45	1.15	500	450	350	0	380

biferrocenylenium-triiodide									
compd	Δ_1 [cm^{-1}]	Δ_2 [cm^{-1}]	λ_1	λ_2	λ_3	λ_4	ζ [cm^{-1}]	Γ_{300K} [cm^{-1}]	Γ_{10K} [cm^{-1}]
$Fc{=}Fc^{\bullet+}I_3$	6650	7650	−2.30	0.90	−0.65	0.95	700	900	800

close to the λ_2 value. Intrinsically, the electronic coupling of the d_{z^2} states is very small and thus has been neglected in the zeroth order; the observable electronic splitting is therefore due to configuration interaction with the $d_{x^2-y^2}$ states ($\zeta = 700$ cm^{-1}). Nevertheless, electronic coupling remains weak, and vibronic coupling leads to two minima along this coordinate. The d_{z^2} exited states are therefore localized, in contrast to the $d_{x^2-y^2}$ ground state (Figure 5). Coupling coefficients for the symmetric Q_{AB} mode ($\lambda_1 = -2.00$ and $\lambda_3 = -0.55$) differ considerably more between the $d_{x^2-y^2}$ and the d_{z^2} exited states than their Q_- counterparts. This can again be explained by consideration of the involved orbitals: the $d_{x^2-y^2}$ combinations have bonding/antibonding character with respect to the metallocene−metallocene bond, leading to a strong coupling in the Q_{AB} mode. The d_{z^2} combinations, in contrast, are nonbonding with respect to this bond, leading to a much weaker coupling in this mode.

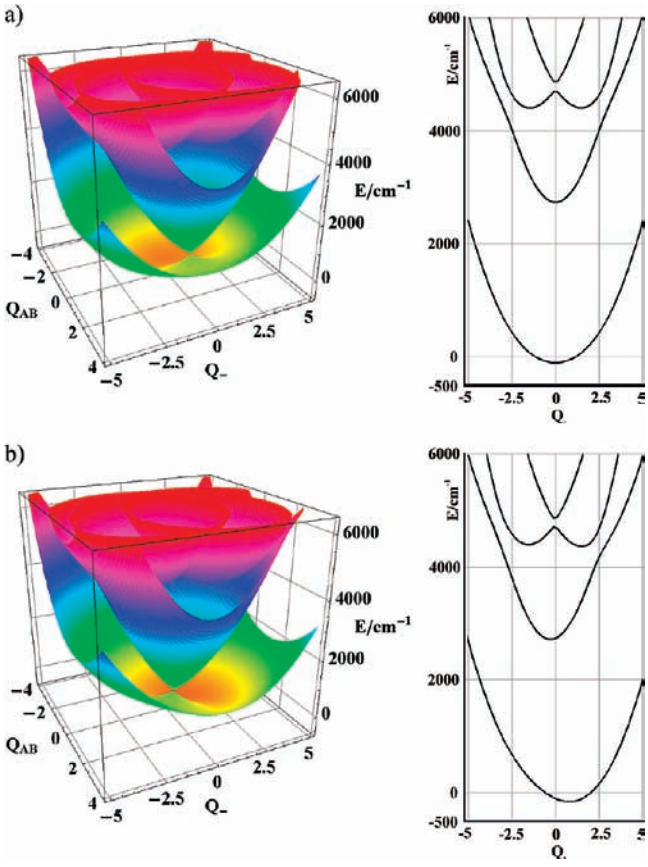

Figure 5. (Left) Three-dimensional representation of the potential energy surface resulting from the four-state VCCI simulation for ferrocenyl ferrocenium triiodide (**1**). Asymmetry following Gasyna and Schatz at (a) $T = 300$ K and (b) $T = 10$ K. (Right) Two-dimensional cuts along Q_- for $Q_{AB} = 0$, see Table 1 for details.

At low temperatures, a satisfactory description of the spectra is only possible using temperature-dependent parameters. Since vibronic and electronic coupling interactions are orbital properties, the corresponding parameters should not be affected by temperature. We therefore exclusively use a temperature-dependent asymmetry to account for the temperature dependence of the spectra. As a result, we obtain an asymmetry parameter of $R = 0.14$ at 10 K. This leads to a single minimum in the potential energy surface displaced along the Q_- coordinate and a maximum at $Q_- = 1.00$ in the probability distribution. For the d_{z^2} exited states, this asymmetry is less pronounced due to the smaller electronic interaction of these states. It has to be noted, however, that the intensity decrease of the integral absorption implied by the asymmetry is not reflected in the spectra; that is, the simulated band shape is below the experimentally measured one, keeping all room-temperature parameters (except R) constant. Possible reasons for this discrepancy are considered in the discussion. In order to arrive at an acceptable low-temperature fit, we therefore have to multiply the theoretical band shape by an empirical factor f_I; the fit gives $f_I = 1.19$.

If we introduce the asymmetry using an off-diagonal matrix element (treatment of asymmetry according to PKS), the vibronic coupling parameters have to be modified slightly to give good results at both 300 and 10 K. The resulting spectra are shown in Figure 6; Table 1 gives the corresponding parameters. For the 300 K spectrum, we again get a symmetric probability distribution along Q_-, whereas at low temperatures the maximum is at $Q_- = 0.80$ with $W_2^{As} = 350$ cm^{-1}. Figure 7 shows the resulting potential surfaces. Again, it is seen that the ground state is delocalized, whereas the excited state is localized. However, for the excited state, the effect of asymmetry is much more pronounced in the PKS formalism than in the Gasyna and Schatz treatment.

For the alkylated compound **(FcEt)$_2$I$_3$** (**2**), we obtain similar vibronic coupling parameters to those for the parent, unsubstituted compound in order to fit the experimental spectra (cf. Figure 8 and Table 1). The IVCT band Ib is of lower intensity as compared to band Ia in this case, which is reflected by a smaller configuration interaction constant of $\zeta = 500$ cm^{-1} in the framework of the VCCI model. This requires a larger spacing Δ_2 between the exited states and the ground state, as the positions of the IVCT bands Ia and Ib are almost identical to compound **1**. Again, we get substantially better results for the simulation of the low-temperature spectrum using a temperature-dependent asymmetry with $R = 0$ at 300 K and $R = 0.14$ at $T = 10$ K. If the asymmetry is considered following PKS (Figure 9), an asymmetry parameter of $W = 380$ cm^{-1} results, and the separation of the d_{z^2} states Δ_2 has to be enlarged from 2050 to 2450 cm^{-1} in order to reproduce the position of the IVCT band Ib (cf. Table 1; for the potential energy surfaces, see the Supporting Information). To reproduce the intensity at low temperatures, a value of $f_I = 1.06$ is used.

The solid-state absorption spectra of the triiodide salt of the doubly bridged cation, **(Fc=Fc$^{\bullet+}$)I$_3$** (compound **3**), finally, are shown in Figure 10, together with theoretical simulations on the basis of the VCCI model. According to larger splitting of the $d_{x^2-y^2}$ bonding and antibonding combinations with respect to the singly bridged compounds **1** and **2**, the double-peak IVCT band is located at 6370 cm^{-1}, about 2800 cm^{-1} higher in energy than for the latter systems. In combination with a configuration interaction ζ of 700 cm^{-1} and a pronounced coupling of the symmetric Q_{AB} mode, a splitting of $\Delta_1 = 6650$ cm^{-1} results. The large displacement in the symmetric stretching coordinate ($\lambda_1 = -2.3$) may again be explained by the fact that an electron is transferred from the cp−cp bonding MO to the antibonding combination (cf. Figure 11); compared to the singly bridged compounds, the covalency is larger, leading to a stronger coupling in Q_1. Vibronic coupling constants in the antisymmetric mode, on the other hand, are comparable to those found for the singly bridged analogs. In contrast to the latter systems, the spectra of the doubly bridged dimer **3** can be fitted at all temperatures without an asymmetry parameter, indicating that a symmetric (and delocalized) electron distribution is always present.

4. Discussion

In the preceding sections, a VCCI model has been developed and applied to the IVCT spectra of the mixed-valent compounds biferrocenyl triiodide **Fc$_2$I$_3$** (**1**), 1′,1‴-diethyl biferrocenyl triiodide (**(FcEt)$_2$I$_3$**; **2**), and Fe(II)/Fe(III) bisfulvalenide triiodide (**(Fc=Fc$^{\bullet+}$)I$_3$**; **3**). The VCCI model is based on the well-known PKS model of vibronic coupling

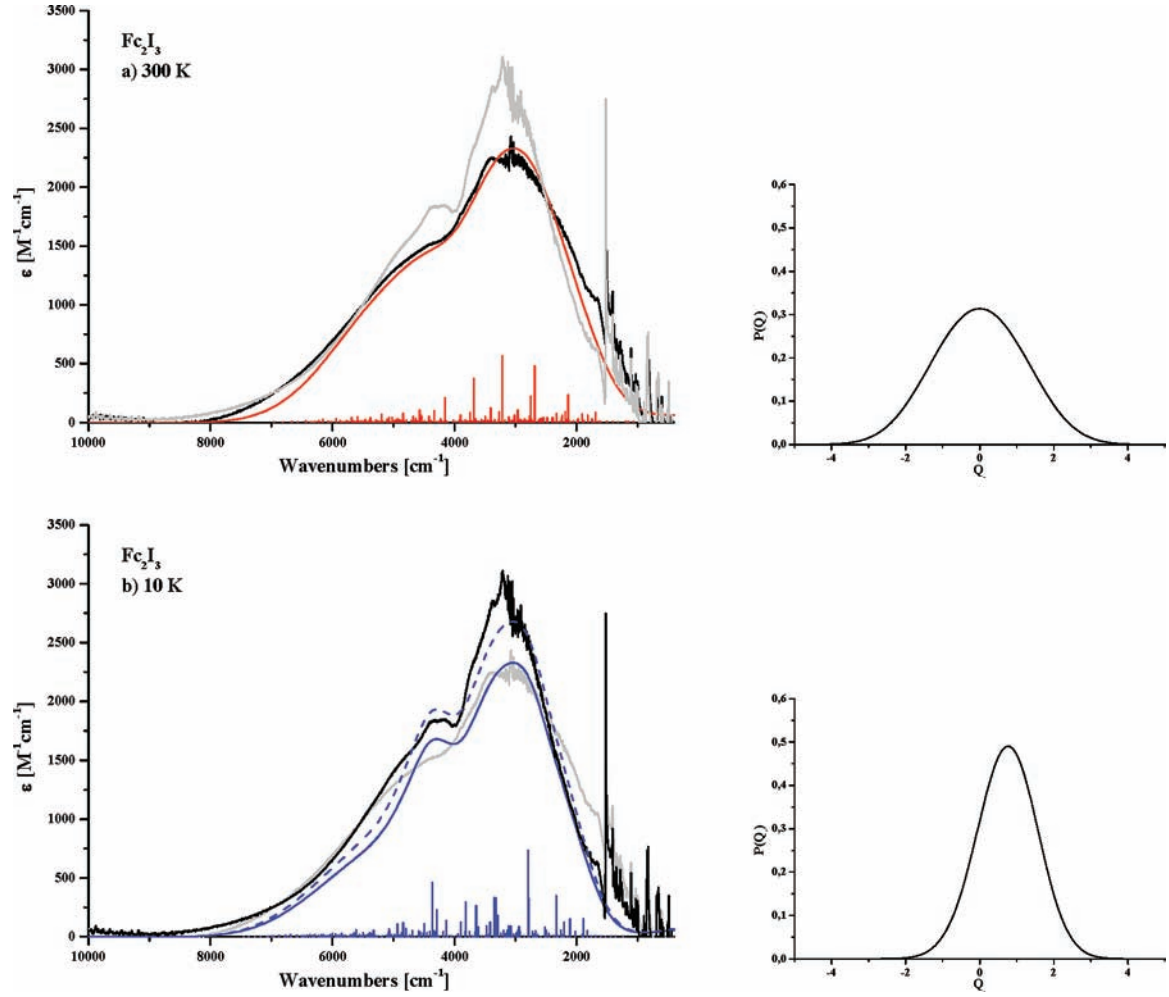

Figure 6. Low-energy optical band of biferrocenyl triiodide (**1**) with theoretical fits (treatment of asymmetry following PKS). (a) $T = 300$ K (black: experimental spectrum; red: theoretical spectrum; gray: experimental spectrum at 10 K) and (b) $T = 10$ K (black: experimental spectrum; blue: theoretical spectrum; dashed blue: theoretical spectrum scaled by $f_I = 1.15$; gray: experimental spectrum at 300 K). Right: probability distribution ($P(Q_-)$). See text and Table 1 for details.

developed by Piepho et al.[17] and incorporates several generalizations of this model that are contained either in its original version or in later modifications.[22,24,31] In particular, the VCCI model includes four electronic states which are connected via configuration interaction. Moreover, it involves two active vibrations, the Q_{AB} and the Q_- modes, and asymmetry. Like the PKS model, the VCCI model allows the explicit evaluation of energies and wave functions and the simulation of the optical absorption spectra of mixed-valence compounds. In addition, it delivers vibronic coupling constants and electronic interaction parameters which allow an estimate of the degree of localization versus delocalization of the investigated systems.

The parameter set of the VCCI model involves four vibronic coupling parameters, λ_1, λ_2, λ_3, and λ_4, the first two of which describe the coupling of the electronic ground state with the first excited state via the $Q_1 = Q_{AB}$ and the $Q_2 = Q_-$ modes, respectively. The second two, λ_3 and λ_4, refer to the horizontal displacement of the two higher-energy d_{z^2} excited states with respect to the $d_{x^2-y^2}$ ground state and vibronic coupling within the d_{z^2} excited states, respectively (cf. Scheme 3). Electronic interaction parameters are Δ_1, Δ_2, and ζ, representing the orbital energy differences (electronic splittings) and the CI interaction parameter within the four-level system, respectively. Taken together, the vibronic coupling parameters and the electronic interaction constants allow for an assessment of the degree of valence localization/delocalization both in the ground and in lowest-energy excited states of the investigated ferrocene−ferrocenium dimers.

The electronic splitting parameter Δ_1 (~3000 cm^{-1} for **1** and **2** and 6650 cm^{-1} for **3**) may be interpreted as the bonding/antibonding interaction of the $d_{x^2-y^2}$ orbitals over the connecting bridge. Using density functional calculations, this splitting was calculated to be about 2000 cm^{-1} for the singly bridged compounds and 4000 cm^{-1} for the doubly bridged ferrocenylene ferrocenylenium cation.[19] The parameter Δ_2, on the other hand, is identified with the separation of the set of d_{z^2} orbitals from the $d_{x^2-y^2}$ ground state. Its value is determined by the VCCI analysis to approximately 5000 cm^{-1} for **1** and **2** and 8100 cm^{-1} for **3**; DFT gave values of about 4000 cm^{-1} (**1** and **2**) and 4500 cm^{-1} (**3**) for this splitting.

When the work of Wong and Schatz is followed,[14] the parameter for vibronic coupling in the PKS mode (the Q_- mode) can be calculated from the difference Δr between the

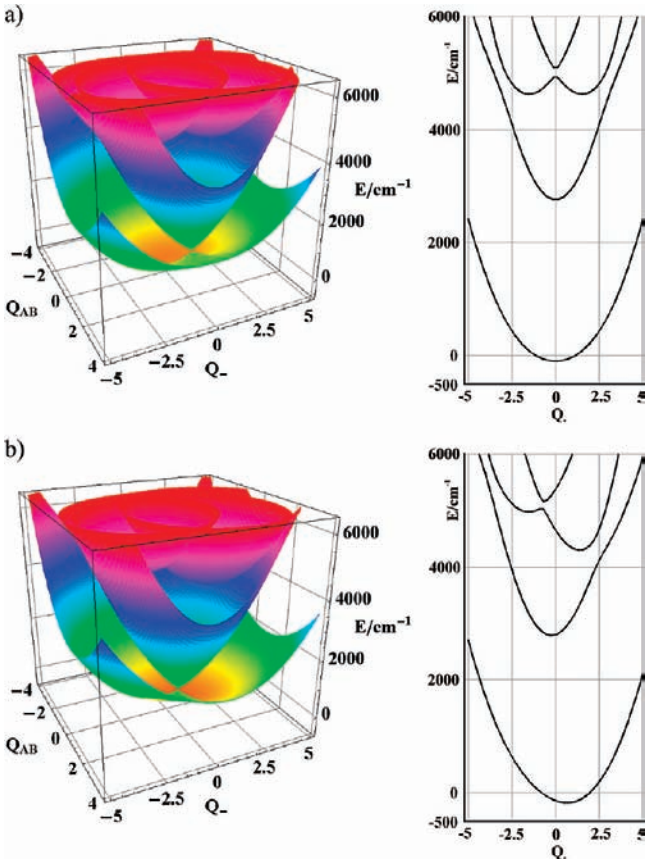

Figure 7. (Left) Three-dimensional representation of the potential energy surface resulting from the four-state VCCI simulation for ferrocenyl ferrocenium triiodide (**1**). Asymmetry following PKS at (a) $T = 300$ K and (b) $T = 10$ K. (Right) Two-dimensional cuts along Q_- for $Q_{AB} = 0$, see Table 1 for details.

equilibrium bond distances of the oxidized and the reduced forms of one subunit:

$$\lambda = 2\Delta r\pi\sqrt{\frac{3\nu_- m_L}{h}} \qquad (45)$$

With a bond length change Δr of 0.04 Å, a frequency ν_- of the Q_- mode of 310 cm^{-1}, and a mass of the ligands (C_5H_5; m_L), of 65 g/mol, a λ_2 value of 1.69 is obtained. The exact determination of the bond length difference of the two oxidation states, however, is not trivial. For example, different values of the cp distances are obtained for different salts. Moreover, ferrocene and its salts partly differ in symmetry. Thus, the staggered conformation is found for the neutral molecule in crystalline matrices, whereas the salts of the ferrocenium cation exhibit a staggered or an ecliptic configuration, depending on the counterion. The determination of vibronic coupling constants via bond length differences thus delivers only approximate values, due to the mentioned difficulties. An alternative approach involves the OVCs introduced by Bersuker et al. (vide supra).

On the basis of the present four-level VCCI model, a value of λ_2 of about 1 is obtained for the coupling of the pseudo-Jahn−Teller active mode Q_- in all three systems. In conjunction with the electronic interaction parameters Δ_1 of about 3000 cm^{-1} for the singly bridged ferrocenyl−ferrocenium salts and about 6650 cm^{-1} for the doubly bridged ferrocenylene ferrocenylenium dimer, *a strong $d_{x^2-y^2}$ ground-state delocalization for the singly as well as doubly bridged ferrocene−ferrocenium dimers* is derived. The d_{z^2} excited states have a slightly larger coupling constant λ_4 in the Q_- mode, about 1.1. These states, however, intrinsically exhibit a weaker electronic interaction, which in the model is neglected at the zeroth order, and only split through configuration interaction with the $d_{x^2-y^2}$ states. Nevertheless, this interaction remains weak, and the parameters thus lead to a double-minimum potential, indicating that *the d_{z^2} excited states are localized*.

Whereas the optical absorption spectra of compound **2** in a polystyrene matrix are almost temperature-independent (data not shown), spectra of **1** and **2** taken in KBr pellets (which contain crystallites of these salts) exhibit a pronounced temperature dependence. In particular, the maximum of the low-energy band Ia shifts to higher energies at low temperatures. This temperature dependence of the solid-state absorption spectra requires the introduction of a temperature-dependent parameter in order to arrive at a satisfying fit at all temperatures. In principle, the high-energy shift of the IVCT band Ia can be accounted for by variation of a number of different parameters. An increased coupling in the Q_- mode, for example, leads to an increased tendency to a double-minimum potential and thus to an increase of transition energies. Depending upon the electronic coupling parameter, however, this does not necessarily lead to a localization at low temperatures: with the remaining parameters kept fixed, the lowest vibrational level would also lie for an increased coupling parameter of $\lambda_2 = 1.5$ *above* the barrier of the potential energy, such that the system would still be delocalized at low temperatures. This result, however, would be in contradiction with the localization observed by Mössbauer spectroscopy at low temperatures.[3] An increase of the electronic interaction parameter Δ_1, on the other hand, could cause a shift of the low-energy band as well. However, the increased electronic interaction would lead to stronger delocalization of the system, again in contradiction with the observed localization at low temperatures. Another parameter that potentially influences the energy of the IVCT transition is the symmetry of the potential along the Q_- coordinate: an asymmetric potential leads to a shift of the absorption band toward higher temperatures; at the same time, a localization of the system is achieved at low temperatures, in agreement with the experimental observation. Simulations of the spectra with a temperature-*independent* asymmetry, on the other hand, did not lead to satisfying fit results. Consequently, the theoretical spectra were simulated with the option of a temperature-dependent asymmetry, in agreement with the Mössbauer data.

Inclusion of asymmetry in the framework of the four-level VCCI was achieved by two approaches described in the literature: the first one already outlined in the original PKS paper is based upon an off-diagonal matrix element in the vibronic matrix;[17] the other one developed by Gasyna et al. involves configuration interaction[24] of the electronic states by a low-symmetry distortion. When the two approaches are

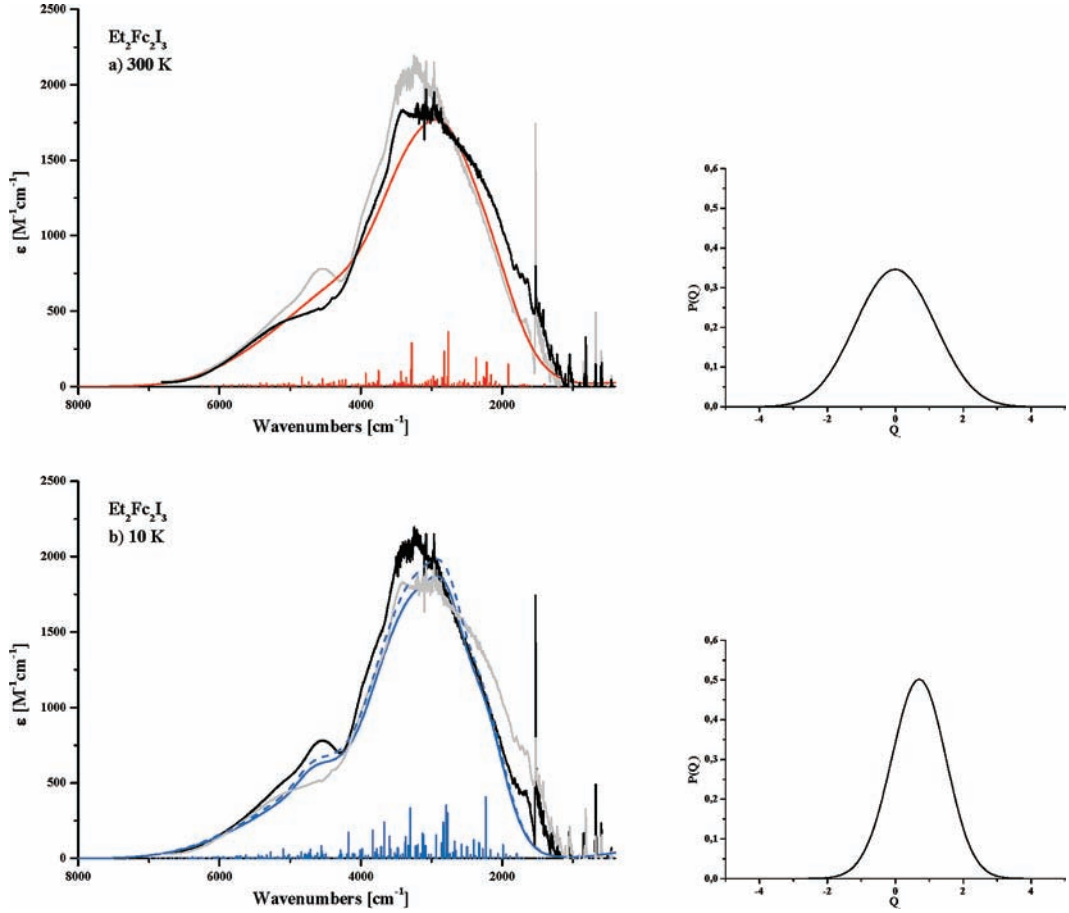

Figure 8. Low-energy optical band of 1′,1‴-diethylferrocenyl ferrocenium triiodide (**2**) with theoretical fits (treatment of asymmetry following Gasyna and Schatz). (a) $T = 300$ K (black: experimental spectrum; red: theoretical spectrum; gray: experimental spectrum at 10 K) and (b) $T = 10$ K (black: experimental spectrum; blue: theoretical spectrum; dashed blue: theoretical spectrum scaled by $f_I = 1.06$; gray: experimental spectrum at 300 K). Right: probability distribution ($P(Q_-)$). See text and Table 1 for details.

compared, it has to be stated that the last approach is in principle preferable, as it employs the *already perturbed* electronic basis states for solution of the dynamic problem, thus being more exact than the former approach, which treats the low-symmetry perturbation *along with* the dynamic problem.[21] Nevertheless, this is also done by the VCCI model, which treats configuration interaction simultaneously with vibronic interactions, such that both approaches are considered on an equal basis in the present study.

In the framework of the VCCI model, the different treatments of asymmetry in particular influence the higher-lying d_{z^2} states 3 and 4. In terms of the Gasyna and Schatz treatment, configuration interaction mixes the original molecular orbitals, leading to new MOs and corresponding electronic states. In the case of a vanishing electronic interaction, Δ, between the subunit basis states, however, configuration interaction between the symmetric and antisymmetric wave functions merely leads to a *localization* but not to an *asymmetry* in the potential. Consequently, a significantly reduced asymmetry is observed in the framework of the Gasyna and Schatz formalism for excited states 3 and 4 as compared to the electronic ground state. In the PKS treatment of asymmetry, this tendency is less pronounced.

The physical interpretation of asymmetry in the case of ferrocene−ferrocenium dimers is a cooperative elastic interaction which leads to a static distortion of the dimer in a crystalline matrix. This phenomenon has also been evidenced in other physicochemical and spectroscopic analyses of this class of compounds.[3] The asymmetry of the crystalline environment influences the ground state as well as the excited state of the individual dimers to a degree which depends upon the sensitivity of these states with respect to a static distortion. Correspondingly, the asymmetry parameters W_i^{As} in the PKS treatment of asymmetry are scaled by the corresponding vibronic coupling constant (cf. eq 40).

Effectively, the two different methods for the inclusion of asymmetry more influence the potential surfaces than the resulting spectra. Simulation of the IVCT spectra with both methods yields comparable parameters of the vibronic coupling parameters, for both the molecular Q_{AB} and the antisymmetric Q_- modes, and agreement of the simulated spectra with the experimental data is comparable for both models as well. Both with the Gasyna and Schatz and with the PKS treatment of asymmetry, however, the predicted total intensity decreases at low temperatures, in disagreement with the experimental observation. The reason for this finding is not obvious. Possibly there are also effects due to asymmetry which lead to an increase of the IVCT intensity and which are not included in the four-state active space of the model (e.g., mixing with LMCT or MLCT states)[19] such that in total an almost temperature-independent integrated intensity could result. So far, however, this hypothesis cannot be

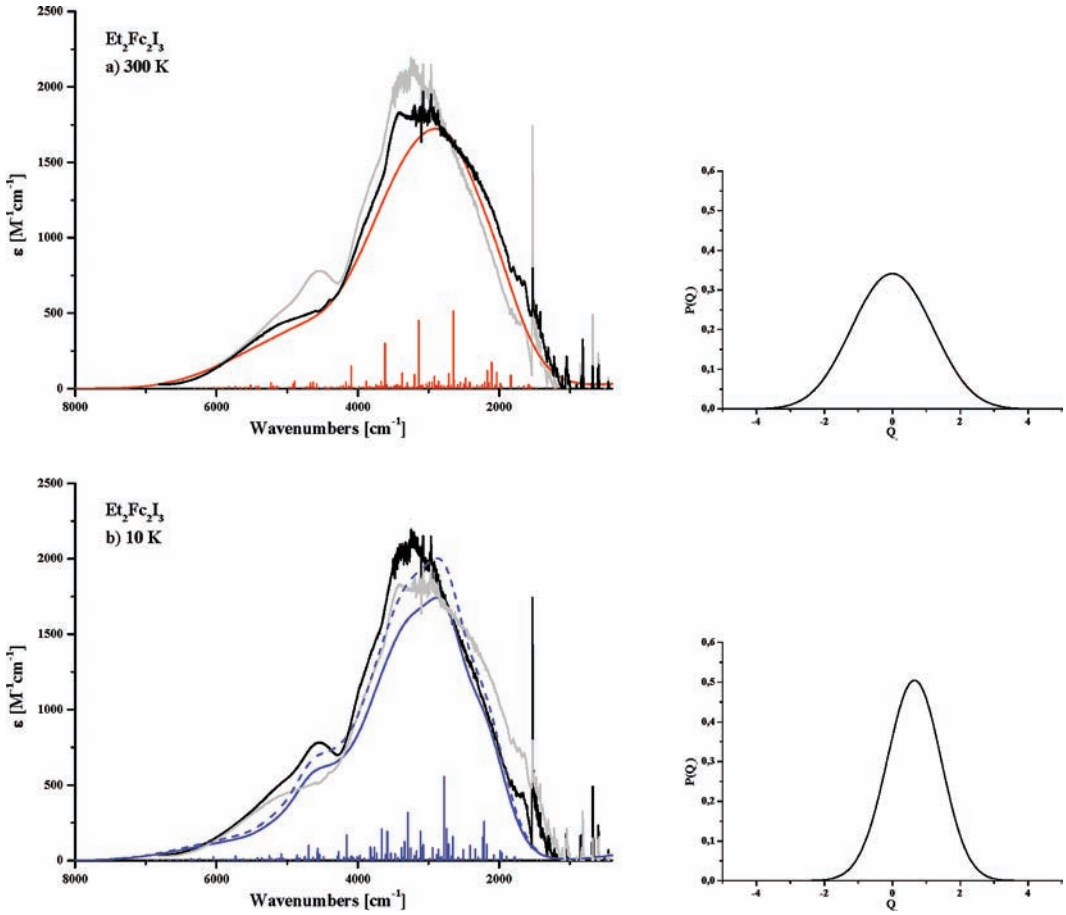

Figure 9. Low-energy optical band of 1′,1‴-diethylferrocenyl ferrocenium triiodide (**2**) with theoretical fits (treatment of asymmetry following PKS). (a) $T = 300$ K (black: experimental spectrum; red: theoretical spectrum; gray, experimental spectrum at 10 K) and (b) $T = 10$ K (black: experimental spectrum; blue: theoretical spectrum; dashed blue: theoretical spectrum scaled by $f_I = 1.15$; gray: experimental spectrum at 300 K). Right: probability distribution ($P(Q_-)$). See text and Table 1 for details.

checked experimentally. Unfortunately, very little experimental information is available on the temperature dependence of IVCT bands. Theoretically, the integrated absorption can increase or decrease slightly, but generally the temperature dependence of IVCT band intensities is predicted to be weak.[14] In the context of this paper, the temperature dependence therefore has been accounted for by an empirical factor f_I, which takes values of about 1.04−1.19 for compounds **1** and **2** at 10 K ($f_I \equiv 1$ at 300 K). For compound **3**, which is delocalized at all temperatures, no asymmetry has to be invoked, and the total absorption intensity is always matched by the theoretical simulation.

The results of the VCCI analysis of **1**−**3** can now be correlated with the solvent shifts determined in the previous study.[19] Just as in the solid state, spin and charge may localize to some degree in one of the two Fc moieties of **1** and **2** in polar solvents, such that the "charge resonance" transitions (cf footnote 20) acquire some charge transfer character and thus become sensitive to solvent polarity. This would be compatible with the notion of biferrocenyl cations as class II/III borderline cases.[34] Moreover, the solvent shift of band Ib may be attributed to the fact that the excited state attained in this transition is subject to a "sudden polarization", such as it occurs on twisting of totally symmetric excited states of polyenes.[35] These two factors would explain the observation of solvent shifts and, in conjunction with the different nature of the excited states, would also account for the fact that the solvent dependence of the IVCT band Ia is weaker than that of band Ib: thus, for band I, excitation would proceed from an almost delocalized bonding to an almost delocalized antibonding molecular orbital; the corresponding dipole moment change and solvent dependence are therefore weak. In case of band Ib, the excitation would proceed from an almost delocalized, bonding molecular orbital into a *localized* orbital, giving a much larger change of dipole moment and, thus, a larger solvent dependence.

This picture also accounts for the fact that, depending on the matrix and the spectroscopic technique, class III or class II behavior is found for the singly bridged dimers **1** and **2**. As already indicated, on the basis of their potentials in the Q_- coordinate, these systems have to be considered as class III (fully delocalized). If localization is observed, it is due

(33) Modifications of the original Gasyna and Schatz programs referenced in ref 21 were used.
(34) D'Alessandro, D. M.; Keene, F. R. *Chem. Soc. Rev.* **2006**, *35*, 393.
(35) (a) Viel, A.; Krawczyk, R. P.; Manthe, U.; Domcke, W. *Angew. Chem., Int. Ed.* **2003**, *42*, 3434 and refs cited therein; (b) Bonačić-Koutecký, V.; Čižek, J.; Döhnert, D.; Koutecký, J. *J. Chem. Phys.* **1978**, *69*, 1168.

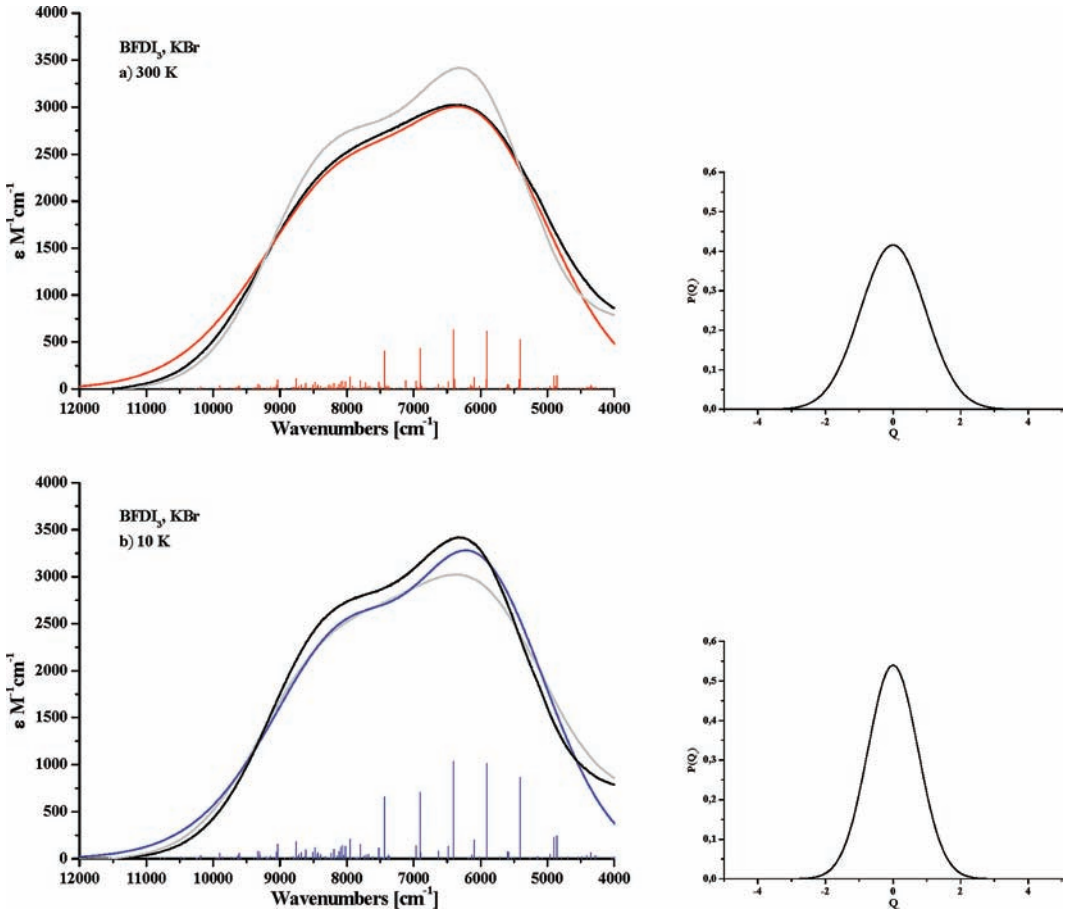

Figure 10. Simulation of the low-energy optical band of ferrocenylene ferrocenylenium triiodide (**3**) at (a) $T = 300$ K and (b) $T = 10$ K along with probability distribution ($P(Q_-)$). Gray: Other temperature. See text and Table 1 for details.

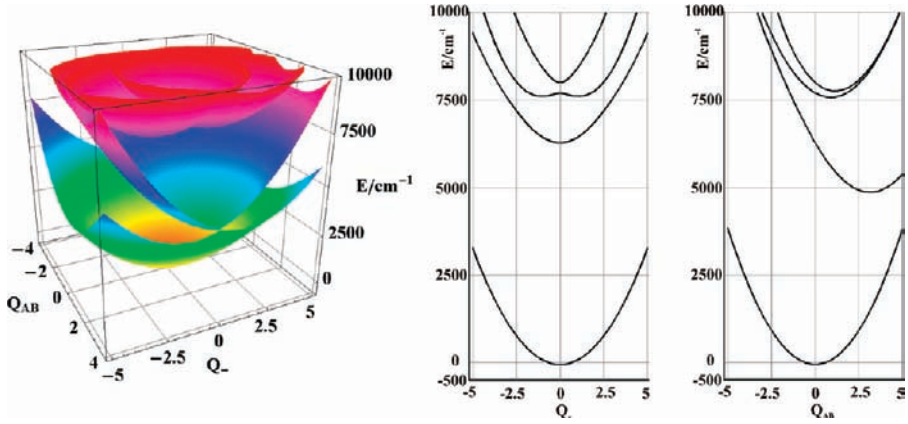

Figure 11. (Left) Three-dimensional representation of the potential energy surface resulting from the four-state VCCI simulation for ferrocenylene ferrocenylenium triiodide (**3**). (Middle) Two-dimensional cut along Q_- for $Q_{AB} = 0$. (Right) Two-dimensional cut along Q_{AB} for $Q_- = 0$, see Table 1 for details.

to an asymmetry in a one-minimum potential and not, as usual, to a double-minimum potential in Q_-. Obviously, the singly bridged dimers **1** and **2** are highly susceptible to dipolar or elastic interactions leading to such asymmetric charge distributions, explaining the class II−III borderline behavior of these compounds observed experimentally. The doubly bridged dimer **3**, in contrast, appears to be inert to such distortions and thus behaves as a class III system under all circumstances.

Relationship to Other Multilevel Models of Mixed-Valence Dimers. There have been other attempts in the literature to incorporate more than one orbital on each subunit of a mixed-valent dimer in a vibronic interaction model to fit the observed IVCT transition band shape. Specifically, Piepho and co-workers[36] and Ondrechen et al.[27−29] included more than one t_{2g} orbital on each of the

(36) Neuenschwander, K.; Piepho, S. B.; Schatz, P. N. *J. Am. Chem. Soc.* **1985**, *107*, 7862.

Scheme 3. Schematic Representation of the Four-State Vibronic Coupling Configuration Interaction (VCCI) Model with Splitting Parameters and Electronic/Vibronic Interaction Parameters

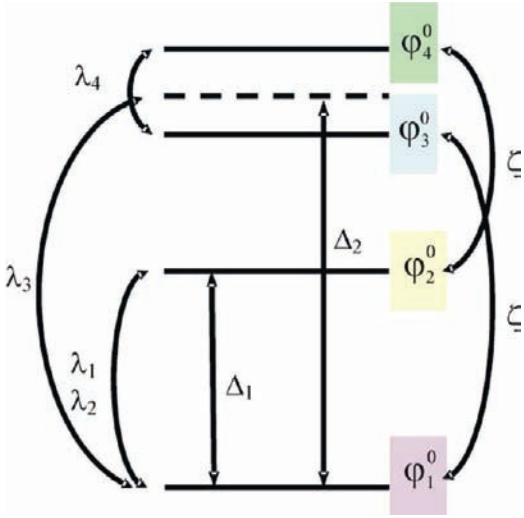

two Ru centers in the Creutz−Taube ion in order to theoretically simulate the observed IVCT band shape. On the basis of the resulting electronic structure, Borshch and Kotov calculated the adiabatic potentials of the complex.[37,38] In all of the mentioned treatments of the Creutz−Taube ion, mixing of the subunit d orbitals was assumed to be mediated by spin−orbit coupling. In the vibronic coupling model of the present paper, in contrast, mixing of the d orbitals is induced by the dimer interaction. Specifically, dimer formation lowers the symmetry of each ferrocene subunit from D_{5h} or D_{5d} to C_{2v}, thus leading to a mixing of $d_{x^2-y^2}$ and d_{z^2}. This mixing, which has also been evidenced by DFT calculations,[19] gives intensity to (formerly forbidden) transitions of $d_{z^2} \rightarrow d_{x^2-y^2}$ character and in the mixed-valent dimer leads to the second component of the observed IVCT band (band Ib). As the mentioned orbitals do not mix by spin−orbit coupling, the latter mechanism cannot account for the two-component character of the IVCT transition in ferrocene−ferrocenium dimers, in contrast with the Creutz−Taube ion. This is different for the pair of $d_{x^2-y^2}$ and d_{xy} orbitals, which in fact can mix by spin−orbit coupling. DFT and TD-DFT calculations on the mixed-valent dimer,[19] however, have shown that the $d_{xy} \rightarrow d_{x^2-y^2}$ IVCT transition is at the *low*-energy side of the dominant IVCT transition of $d_{x^2-y^2} \rightarrow d_{x^2-y^2}$ character (band Ia) and thus cannot account for the existence of the second transition at the *high*-energy side of this absorption band (band Ib).

Relationship to the Bacterial Photosynthetic Reaction Center. The vibronic treatment of asymmetric dimers developed by Gasyna and Schatz and adopted in the present paper was also applied by these authors to the bacterial photosynthetic reaction center.[39] Importantly, the oxidized form of this reaction center, $P^{\bullet+}$, represents an asymmetric mixed-valent dimer and exhibits an IVCT band which, although of totally different electronic origin, is quite similar in appearance to the IVCT band detected for the biferrocenyl radical cations. In particular, it consists of a broad and somewhat structured electronic absorption feature and, on the low-energy side, a large number of sharp infrared absorption peaks, so-called phase-phonon lines.[40] Moreover, in the overlap region between the sharp absorption lines and the broad electronic absorption, intense lines exhibiting a derivative line shape are observed. Such features are termed Fano (or antiresonance) lines[41] and appear when a sharp line is overlapped by a broad continuum-like absorption from another transition. Gasyna and Schatz have simulated both the phase-phonon and the broad electronic absorption region of the $P^{\bullet+}$ radical cation with a two-level, two-mode model including asymmetry and also attempted to fit the Fano lines with a dispersion-like band shape.[39] Interestingly, the low-energy spectra of ferrocene−ferrocenium dimers also reveal the presence of phase-phonon as well as Fano lines, besides the broad electronic absorption band. We have not attempted to fit the sharp-line features of our spectra but want to stress that these features are not noise (as they are observed at identical positions in different samples) but contain spectroscopic information which needs to be accounted for in a more complete treatment.

A suitable theoretical framework to achieve this has been developed and applied to the oxidized photosynthetic reaction center by Reimers et al.[42−44] These authors have outlined a protocol to describe the electronic/vibronic structure and simulate the phase-phonon and IVCT region of $P^{\bullet+}$ as well as the corresponding Stark spectra.[45−48] Closer analysis of the IVCT absorption feature reveals the presence of a second transition, which needs to be included in a theoretical treatment in order to arrive at a satisfactory fit of the overall band shape. Specifically, $P^{\bullet+}$ consists of two bacteriochlorophyll units, each of which has a highest-energy MO (HOMO) approximately corresponding to the porphyrin b_{1u} orbital and a second-highest MO (SHOMO) approximately corresponding to a porphyrin orbital of a_u symmetry.[42] In the dimer, both HOMO and SHOMO split into a pair of symmetric/antisymmetric combinations transforming, respectively, as "a" and "b" in the C_2 point group of the special pair. The electronic structure of the mixed-valent dimer thus can be described by a three-electron, four-level scheme:[43] the ground state (GS) $(1)^2B$ has a hole in the "b" combination of the monomer HOMOs, and the "hole-transfer" (HT) state

(37) Borshch, S. A.; Kotov, I. N. *J. Struct. Chem.* **1991**, *32*, 35–39.
(38) (a) Bersuker, I. B. *Electronic Structure and Properties of Transition Metal Compounds. Introduction to the Theory*; John Wiley & Sons: New York, 1996. (b) Bersuker, I. B. *Adv. Chem. Phys.* **1992**, *81*, 703.
(39) Gasyna, Z.; Schatz, P. N. *J. Phys. Chem.* **1996**, *100*, 1445–1448.
(40) (a) Rice, J. *Phys. Rev. Lett.* **1976**, *37*, 36. (b) Rice, J.; Lipari, N. O.; Strässler, S. *Phys. Rev. Lett.* **1977**, *39*, 1359. (c) Rice, M. J. *Solid State Commun.* **1979**, *31*, 93. (d) Rice, M. J.; Yartsev, V. M.; Jacobsen, C. S. *Phys. Rev. B: Condens. Matter Mater. Phys.* **1980**, *21*, 3437.
(41) Sturge, M. D.; Guggenheim, H. J.; Pryce, M. H. L. *Phys. Rev. B: Condens. Matter Mater. Phys.* **1970**, *2*, 2459.
(42) Reimers, J. A.; Shapley, W. A.; Hush, N. S. *J. Chem. Phys.* **2003**, *119*, 3240.
(43) Reimers, J. A.; Shapley, W. A.; Rendell, A. P.; Hush, N. S. *J. Chem. Phys.* **2003**, *119*, 3249.
(44) Reimers, J. A.; Hush, N. S. *J. Chem. Phys.* **2003**, *119*, 3262.
(45) Treynor, T. P.; Andrews, S. S.; Boxer, S. G. *J. Phys. Chem. B* **2003**, *107*, 11230.
(46) Treynor, T. P.; Boxer, S. G. *J. Phys. Chem. A* **2004**, *108*, 1764.
(47) Treynor, T. P.; Boxer, S. G. *J. Phys. Chem. B* **2004**, *108*, 13513.
(48) Kanchanawong, P.; Dahlbom, M. G.; Treynor, T. P.; Reimers, J. R.; Hush, N. S.; Boxer, S. G. G. *J. Phys. Chem. B* **2006**, *110*, 18688.

$(1)^2$A has a hole in the corresponding "a" combination. In addition, there exists an "SH" state, $(2)^2$B, having a hole in the "b" combination of the monomer SHOMOs and a "HTSH" state, $(2)^2$A, having a hole in the corresponding "a" combination. The two splitting schemes are interlocked in such a way that an energy sequence GS < SH < HT < HTSH results. As a consequence, in addition to the strongly allowed GS → HT band, transitions involving the (in the monomer forbidden) SHOMO→ HOMO excitation can occur in the mixed-valent dimer.

Importantly, the intensity of the (in the monomer forbidden) GS → SH transition has been assumed by Reimers and Hush to be mediated by a Herzberg−Teller mechanism whereby the forbidden GS → SH transition "steals" intensity from the intense GS → HT transition through a vibronic HT ↔ SH interaction.[44,49,50] The same type of interaction has been postulated between the GS and the HTSH states. In contrast, electronic mixing (CI) between states of like symmetry (GS ↔ SH (both of ^{2}B symmetry) and HT ↔ HTSH (both of ^{2}A symmetry)) has been neglected by these authors. This implies that the GS → HTSH transition (although being of ^{2}B → ^{2}A type, as the intense GS → HT transition) has no *intrinsic* electric-dipole intensity. As experimentally the intensity of this transition is in fact found to be very weak,[48] this approximation appears to be justified for the PRC.

In our treatment of the biferrocenyl radical cation, in contrast, vibronic coupling between $d_{x^2-y^2}$ and d_{z^2} states of *unlike* symmetry is neglected, and the CI between $d_{x^2-y^2}$ and d_{z^2} states of *like* symmetry is considered as the only mechanism of intensity borrowing. As a consequence, one of the (in the monomer-forbidden or very weak) transitions of d_{z^2} → $d_{x^2-y^2}$ character acquires *intrinsic* electric-dipole intensity in the dimer (band Ib), which does *not* depend upon a Herzberg−Teller mechanism. This is in full agreement with results from TD-DFT calculations performed in the preceding paper,[19] which indicate the presence of *two* IVCT transitions of comparable intensity. On the other hand, we cannot account for a possible intensity increase of the parity-(electric-dipole) forbidden component of the d_{z^2} → $d_{x^2-y^2}$ transition by Herzberg−Teller coupling, as this mechanism is not included in our model. This might also be one reason for our lack of perfectly reproducing the temperature dependence of the spectra (vide supra).

5. Conclusions

In the present paper, a four-level, two-mode vibronic coupling scheme including asymmetry has been formulated and applied to the IVCT bands of ferrocene−ferrocenium dimers. The main emphasis has thereby been laid on the two singly bridged biferrocenyl radical cations and the interpretation of their IVCT transitions. Although no perfect agreement with the experimental band shape could be obtained and the temperature dependence of the integrated absorption was not quantitatively reproduced, a qualitative understanding of the unusual band shape as well as its relationship with the asymmetric distortion of these dimers evidenced by other spectroscopies was achieved. Clearly, more work is required to arrive at a deeper understanding of the low-energy transitions of these dimers, including the phase-phonon region. The present paper should be considered as a first step in this direction; more advanced theoretical methods like that applied by Reimers and Hush to the photosynthetic reaction center or alternative experimental techniques like Stark spectroscopy (vide supra) might be required to fully and systematically understand the low-energy transitions exhibited by these systems, including the temperature dependence of the IVCT bands and the influence of asymmetric distortions imposed by the surrounding medium on their bandshapes.

Acknowledgment. F.T. thanks Christian Albrechts University Kiel for funding of this research.

Supporting Information Available: Additional discussion, figures, and tables. This material is available free of charge via the Internet at http://pubs.acs.org.

IC802112H

(49) Reimers, J. R.; Hush, N. S. *J. Am. Chem. Soc.* **2004**, *126*, 4132.
(50) Reimers, J. R.; Hush, N. S. *Chem. Phys.* **2004**, *299*, 79.